NTNU

Norwegian University of
Science and Technology

Wet Gas Compression
Impeller Rig

Siren Carstens Amundsen

Problem Description

The overall scope of the thesis is to document compressor performance and stability for single- and multiphase compression.

Assignment given: 09. February 2009
Supervisor: Lars Erik Bakken, EPT

Preface

This report contains the work performed on my master thesis at the Norwegian University of Science and Technology, Department of Energy and Process Engineering. The work was conducted during the spring of 2009.

I would like to thank Professor Lars E. Bakken, PhD Øyvind Hundseid and PhD graduate student Trond G. Grüner for valuable guidance throughout my work.

Trondheim, July 6th 2009

Siren Carstens Amundsen

Siren Carstens Amundsen

Abstract

Wet gas compression technology is of great value to the oil and gas industry for boosting of unprocessed well stream and to reduce investment costs related to equipment and personnel. The growing interest in wet gas compression leads to a general request for accurate performance calculation procedures and proper measurement techniques for multiphase flow metering in compressors.

An impeller rig for examination of single-phase and multiphase performance and aerodynamic stability is under construction at the test facility at NTNU. The construction of the compressor rig is behind time due to late deliveries of the compressor components and instrumentation. The performance calculations are therefore based upon one compressor test conducted with dry gas at part-load.

The thermodynamic equation of state for ambient air is verified to be consistent with the ideal gas law in the compressor pressure and temperature range. The calculated polytropic performance is calculated with ideal gas assumptions and compared to values estimated by PRO/II. By analyzing the results the sensitivity of the calculation procedures is identified and the suitability for the ideal polytropic performance calculations is validated for the actual compressor test and operating range.

A sensitivity analysis is conducted in order to determine the effect of measurement uncertainties on performance calculations. Due to the low pressures involved for the compressor test, the performance calculation procedures are highly sensitive to uncertainties in the pressure measurements. Uncertainties in the temperature measurements will only slightly influence the polytropic head, but have great influence on the polytropic efficiency.

The efficiency and operating range of a compressor are constrained by aerodynamic instabilities. This thesis describes the different flow phenomena associated with compressor instability and presents recommendations for suitable instrumentation and measuring techniques. Various visualization techniques are in addition evaluated to determine the suitability for multiphase compressors.

Dynamic pressure transducers installed in the inlet and discharge piping are recommended for detection of pressure pulsation throughout the compressor system. Unsteady internal pressure measurements can be obtained from circumferentially distributed pressure transducers at various locations within the compressor components. Vibration probes installed at each end of the rotor are recommended for the vibration measurements. By analyzing the frequency spectrum for the pressure fluctuation and radial vibrations one can identify the type of instability phenomenon that occur. Laser measurement techniques are recommended for the flow visualization in order to obtain information on the main features of the multiphase flow field.

Abstract in Norwegian

Sammendrag

Våtgass kompresjon er en relativt ny teknologi som olje og gassprodusentene ønsker å utvikle for å kunne øke trykkstøtten til eksisterende felt. Trykkstøtte til produktive brønner gir direkte fortjeneste ved akselerert produksjon og ved redusering av utstyr og bemanning. En stadig økende interesse for våtgass teknologi har resultert i et behov for nøyaktige beregninger av ytelse og egnede måleteknikker for flerfase strømning i kompressorer.

Eksperimentell forsøksrigg for undersøkelse av ytelse og aerodynamisk stabilitet for en- og flerfase kompresjon er under oppføring ved NTNU. Grunnet forsinkelser i leveranser og oppføringen av testriggen er det kun gjennomført testing for tørr gass. Ytelsesberegningene er dermed basert på målinger for kun en test for tørr gass med dellast.

Tilstandsligningen for atmosfærisk luft er i overensstemmelse med den ideelle gass lov i operasjonsområdet til kompressoren. Kompressorytelsen er dermed beregnet med ideell polytropisk analyse og sammenlignet med verdier estimert ved simuleringer i PRO/II. Ved analyse av resultatene er sensitiviteten til ytelsesberegningene dokumentert. Bruk av ideell polytropisk analyse er validert for kompressor operasjonsrådet.

Sensitivitet med hensyn til målenøyaktighet er inkludert i analysene. Grunnet lave trykk for kompressortesten er ytelsesberegningene sterkt sensitive for usikkerhet i trykkmålingene. Unøyaktighet i temperaturmålingene vil i liten grad påvirke den polytropiske løftehøyden, men vil ha sterk innvirkning på den polytropiske virkningsgraden.

Kompressor ytelse og dets operasjonsområde er begrenset av aerodynamisk ustabilitet i maskinen. De forskjellige strømningsfenomenene assosiert med aerodynamisk ustabilitet blir beskrevet i denne oppgaven med påfølgende anbefalinger av egnede målemetoder og instrumentering. Ulike visualiseringsteknikker er i tilegg evaluert for bruk ved våtgass kompresjon.

I tilegg til stasjonære målinger i innløps- og utløpsrør, kan målinger av trykk fluktuasjoner implementeres for detektering av aerodynamisk ustabilitet. Dynamiske trykk transmittere med høy respons anbefales for slike målinger. Vibrasjonsfølere på hver side av rotoren anbefales for målinger av radiell vibrasjon. Ved analyse av frekvens spekteret for trykk- og vibrasjonsfluktuasjoner kan aerodynamisk ustabilitet dokumenteres. Lasermålinger er anbefalt for visualisering av strømningen.

Contents

List of Figures

List of Tables

Nomenclature

Symbols

A	Area	[m^2]
a	Speed of sound	[m/s]
C	Discharge coefficient	[-]
D	Diameter	[m]
f	Schultz correction factor	
H	Head	[m]
h	Enthalpy	[J/kg]
I	Intensity	[W/sr]
i	Incidence angle	[°]
Ma	Mach number	[-]
M$_w$	Molecular weight	[kg/kmol]
m	Mass flow rate	[kg/s]
N	Rotational speed	[rpm]
n	Polytropic exponent	[-]
P	Power	[W]
p	Pressure	[Pa]
Q	Volume flow	[m^3/s]
R	Gas constant	[J/kg K]
Re	Reynolds number	[-]
s	Entropy	[J/kg K]
T	Temperature	[K]
U	Tangential velocity	[m/s]
V	Relative velocity	[m/s]
v	Specific volume	[m^3/kg]
X	Schultz compressibility function	
Y	Schultz compressibility function	
Y	Specific work	[J/kg]
Z	Compressibility factor	[-]
α	Gas volume fraction	[-]
β	Beta ratio	[-]
ε	Expansibility factor	[-]
κ	Isentropic exponent	[-]
η	Efficiency	[-]
ρ	Density	[kg/m^3]
μ	Dynamic viscosity	[cP]
τ	Torque	[N*m]
φ	Flow coefficient	[-]
ψ	Head coefficient	[-]
ω	Angular velocity	[1/s]

Subscript

1	Inlet, suction state
2	Outlet, discharge state
c	Critical
g	Gas
l	Liquid
m	Mechanical
max	Maximum
min	Minimum
p	Polytropic
ref	Reference
S	Schultz
s	Isentropic
v	Volume corrected

Abbreviations   **Description**

ASME	American Society of Mechanical Engineers
CCD	Charge-Coupled Device
CFD	Computational Fluid Dynamics
EOS	Equation of State
FFT	Fast Fourier Transformation
GVF	Gas Volume Fraction
ISO	International Organization for Standardization
L2F	Laser two-focus velocimetry
LDV	Laser Doppler Velocimetry
NTNU	Norwegian University of Science and Technology
PIV	Particle Image Velocimetry
PSP	Pressure Sensitive Paint
PTC	Performance Test Code
SI	International System of Units
SM	Surge Margin

Equations of State

BWR	Benedict-Webb-Rubin
BWRS	Benedict-Webb-Rubin-Starling
GERG	University of Bochum (ISO Committee)
LKP	Lee-Kesler-Plocker
PR	Peng-Robinson
RK	Redlich-Kwong
SRK	Soave-Redlich-Kwong

Test rig: the total test assembly including all instrumentation.

Chapter 1

1. Introduction

Chapter 1 explains the background and motivation for the work presented. In addition, the scope of the thesis, limitations and challenges related are presented.

1.1 Background

An experimental impeller rig for examination of single-phase and multiphase performance and aerodynamic stability is under construction at the test facility at NTNU. Accurate measuring results depend on the selection and implementation of proper instrumentation as well as the applicability of the selected performance procedure for the actual compressor test. The instrumentation and performance procedures must satisfy established standards for compressor performance testing in addition to various requirements for detection of aerodynamic instability.

Various applicable performance test codes are available for dry gas compressor testing. ASME PTC 10 [1] provides specific guidelines for accurate measuring procedures in addition to correct installation and location of various measuring devices.

Multiphase flows in compressors have complicated characteristics including interfacial interactions and relative movement between phases. Determination of actual fluid and thermodynamic properties is a challenge in multiphase compressors due to this phase exchange. The instrumentation and measurement techniques employed for single-phase compression may have insufficient accuracy due to the liquid introduced in wet gas compression.

Measurement and visualization techniques with careful control of the flow distribution are desired in wet gas compression to examine the multiphase flow effects under various conditions in the compressor. Most of the compressor testing described in literature is performed utilizing single-phase fluid. Techniques commonly used for visualization of single-phase flow may be difficult to implement in multiphase compressors due to the inherent non-homogeneity of the flow field.

1.2 Scope of Thesis

The overall scope of the thesis is to document compressor performance and stability for single- and multiphase compression. An extensive literature study forms the foundation for planning and conducting single- and multiphase compressor tests. Part of this literature study was presented in the previous work by the author. [2]

The effect of measurement uncertainty on performance calculations is examined to determine the measurement sensitivity.

Various measurement and visualization techniques are investigated to determine the suitability for multiphase compressor testing. By achieving increased understanding of the multiphase effects existing in wet gas compression and the phenomena associated with aerodynamic instability, one can determine an appropriate instrumentation setup and suitable measuring techniques.

1.3 Limitations and Challenges

The construction of the compressor rig was behind time due to late deliveries of the compressor components and instrumentation. The performance calculations are therefore based upon one compressor test conducted with dry gas at part-load. The results can nevertheless be utilized to validate the compressor behavior at the test operating condition.

Instrumentation for detection of compressor instabilities and the injection module for wet gas testing are not yet implemented. Documentation of compressor performance and stability for multiphase compression are therefore discarded from the work presented. Recommended methods, procedures and instrumentation for wet gas is instead presented for future wet gas testing.

1.4 Report Structure

Chapter 2 describes the relevant performance procedures needed to document and validate the performance calculations for the compressor rig.

Chapter 3 presents the theoretical foundation for the test preparation based on various applicable standards and available literature.

Chapter 4 describes the NTNU test facility and documents the experimental instrumentation set up.

Chapter 5 describes the compressor testing and presents the results concluded from the performance analysis.

Chapter 6 shows the effect of measurement uncertainties on the performance calculations for the compressor test.

Chapter 7 gives the theoretical foundation for detection of aerodynamic instabilities in centrifugal compressors. Recommendations for suitable instrumentation are in addition presented.

Chapter 8 presents various measurement and visualization techniques employed in single-phase and multiphase systems and determines the suitability for multiphase compression.

Chapter 9 concludes the results that can be drawn based on the work presented.

Chapter 10 contains recommendations for further work.

Chapter 2

2. Performance Analysis

An accurate method for performance calculations is important to ensure a correct evaluation of the centrifugal compressor. Performance calculations in ASME PTC 10 [1] are based on dry gas compression. In default of correct standards and methods for wet gas compression the test results may deviate considerably when liquid is present in the gas.

The specific work of a compressor is dependent on the compression process and the compressed gas. For comparison, the ideal isentropic compression process can be utilized. By introducing the isentropic condition ($pv^{\kappa}=constant$), the specific isentropic work for a compressor is shown as in equation (2.1).

$$Y_s = Z_1 R T_1 \frac{\kappa}{\kappa-1} \left[\left(\frac{p_2}{p_1} \right)^{\left(\frac{\kappa-1}{\kappa} \right)} - 1 \right] \tag{2.1}$$

The term *head* is generally employed when referring to the specific work done by a compressor. The compressor actual head, equation (2.2), describe the total change in enthalpy for the compression process. The relationship between pressure, temperature and enthalpy are determined by utilizing an appropriate equation of state. The actual head remains constant independently of the given compression process.

$$H = h_2 - h_1 = h(p_2, T_2) - h(p_1, T_1) \tag{2.2}$$

2.1 Polytropic Analysis

The thermodynamic evaluation of centrifugal compressors is generally based on the polytropic procedure. Identical compressors operating at different suction pressures will have variation in isentropic efficiencies due to the deviation in the isobars [$(dh/ds)_p$=T]. This thermodynamic characteristic is taken into account when assuming a polytropic process. The deduction of the polytropic head is based on the assumption of a constant polytropic exponent along the compression path. The compressor polytropic head is given in equation (2.3).

$$H_p = Z_1 R T_1 \left[\frac{n}{n-1} \right] \left[\left(\frac{p_2}{p_1} \right)^{\frac{n-1}{n}} - 1 \right] \tag{2.3}$$

The polytropic efficiency is defined as the relationship between polytropic and actual head as shown in equation (2.4).

$$\eta_p = \frac{H_p}{H} \tag{2.4}$$

Equation (2.5) shows the relationship between the polytropic head, efficiency and compressor power requirement. The mechanical efficiency, η_m, is usually estimated to about 97-98.5 %. [3]

$$P = \frac{\rho_1 Q_1 H_p}{\eta_m \eta_p} \tag{2.5}$$

The definitions and equations utilized in the polytropic calculation procedure are given in Appendix A.1.

2.2 Schultz Polytropic Analysis

At high pressures and temperatures, the ideal gas behaviour is not valid due to changes in fluid properties. Both ASME PTC 10 [1] and ISO 5389 [4] have implemented the John M. Schultz polytropic procedure [5] for thermodynamic performance evaluation of a compressor. Real gas behaviour is taken into account when utilizing the Schultz procedure.

The procedure assumes a polytropic compression path based on averaged gas properties of inlet and outlet conditions. Schultz introduced a polytropic volume exponent, n_v, to account for changes in fluid properties. The polytropic volume exponent is defined as a constant in solving the polytropic head equation due to assumed negligible variation.

The Schultz polytropic head can then be calculated from equation (2.6), where the correction factor, f, is introduced to account for the slight variation in n_v.

$$H_{p,S} = f * Z_1 R T_1 \left[\frac{n_v}{n_v - 1} \right] \left[\left(\frac{p_2}{p_1} \right)^{\frac{n_v - 1}{n_v}} - 1 \right] \tag{2.6}$$

Definitions and equations for the Schultz calculation procedure are given in Appendix A.2.

ASME PTC 10 refers to the Schultz procedure in cases where the outlet conditions are *unknown*. An arithmetic mean value between inlet and outlet conditions is utilized for estimating the compressibility, compressibility function, and the specific heat. This is *not* in accordance with the Schultz procedure, where an imaginary midpoint is utilized for evaluating the exponents and compressibility functions.

2.3 Wet Gas Performance Analysis

The presence of liquid increases the flow complexity in the compressor. Fluid properties may vary through the compression process due to energy transfer between the phases. The dry gas performance analysis becomes insufficient when analysing wet gas compressor performance. [6] A detailed analysis of the fluid properties along the compression path is essential to assure correct calculations. The phase exchange during wet gas compression is not accounted for when utilizing averaged gas properties as in the Schultz procedure.

Direct Integration Analysis

Direct integration of the polytropic process comprehends iteration from suction to discharge conditions as shown in equation (2.7). The assumed polytropic efficiency is kept constant during the iteration process.

$$h_p = \sum_{i=1}^{\infty} \partial h_s \Big|_{\eta_p = \text{constant}} \tag{2.7}$$

The direct integration procedure is independent of the type of fluid being compressed and involves using real gas properties. [7] Phase changes along the compression path are included in the procedure and permit a detailed prediction of the actual volumetric flow through the compressor. The procedure is suitable for wet gas compression and should be applied in wet gas performance analysis where phase changes along the compression path are present. [6] The accuracy of the direct integration performance analysis is dependent

on the validity of the relevant equation of state and the determination of the fluid composition.

2.4 Equation of State

The compressor aerodynamic performance is defined by the enthalpy difference over the compressor. Enthalpies cannot be measured directly and must therefore be determined from an appropriate equation of state. An equation of state, EOS, is a thermodynamic equation describing the mathematical relationship between two or more state functions, such as pressure, temperature and volume.

It is generally not possible to determine the most accurate EOS to predict gas properties. Neither ASME PTC 10 nor ISO 5389 gives recommendations regarding the preferred equation of state for compression processes. The calculated performance may vary depending on the implemented EOS. Frequently used equations of state are Redlich-Kwong (RK), Soave-Redlich-Kwong (SRK), Peng-Robinson (PR), Lee-Kesler-Plocker (LKP), Benedict-Webb-Rubin (BWR) and Benedict-Webb-Rubin-Starling (BWRS).

Equation (2.8) gives the general EOS for a gas, where the compressibility factor, Z, is included to account for compressibility effects.

$$pv = ZRT \tag{2.8}$$

To utilize the general EOS, the compressibility factor must be determined for the specified gas and actual compressor operating range. Equation (2.9) shows a virial EOS that can be derived from the principles of statistical mechanics to relate the p-v-T behavior of a gas to the forces between molecules. The virial coefficients B, C, D, etc. can be determined analytically or from empirical data. The virial equation of state has a strong theoretical foundation and is free of arbitrary assumptions.

$$Z = 1 + \frac{B(T)}{v} + \frac{C(T)}{v^2} + \frac{D(T)}{v^3} + \dots \tag{2.9}$$

At states of a gas where the pressure is small relative to the critical pressure, the second, third and higher terms of equation (2.9) will diminish. The compressibility factor will thus approach unity at fixed temperature, giving the ideal gas equation of state. To verify that a gas can be modeled as an ideal gas, the states of interest must be investigated to determine how well Z=1 is satisfied.

At high pressures and temperatures, the ideal gas behavior is not valid. Changes in fluid properties must be accounted for by implementing an appropriate EOS in the performance calculations. The modified virial equation of state, the BWRS, is recommended by Twu et al. [8] for gases in every temperature and pressure range.

An appropriate equation of state is essential when analyzing wet gas compression due to phase exchanges when liquid is introduced. Phase changes will affect the actual volumetric flow through the compressor and hence the compressor performance validation. The commonly used equations of states are not suitable for prediction of such phase behavior. [8] Hundseid et al [6] demonstrated the suitability for the GERG-2004 equation of state for wet gas applications. The GERG EOS gives accurate density values in both vapor and liquid phases and should therefore be implemented for the wet gas analysis.

2.5 Conclusion Chapter 2

The ideal polytropic performance analysis is suitable for compression processes where the compression fluid behaves approximately like an ideal gas. To verify that a gas can be modeled as an ideal gas, the states of interest must be investigated to determine how well $Z=1$ is satisfied.

At high pressures and temperatures, the ideal gas behavior is not valid. Changes in fluid properties must be accounted for by implementing the Schultz polytropic analysis for performance calculations.

The direct integration procedure is suitable for wet gas performance analysis where phase changes along the compression path are present. Phase transitions in wet gas compression can be assumed negligible at states where the pressures and temperatures are low and the fluid inlet condition is stable.

The accuracy of the various performance calculations is dependent on the validity of the implemented equation of state. The ideal EOS provides an acceptable approximation at states of a gas where the pressure is small relative to the critical pressure, but will be highly inaccurate at states with high pressures and temperatures. The BWRS equation of state is recommended by Twu et al. [8] for gases in every temperature and pressure range. In wet gas compression the GERG EOS gives accurate density values in both vapor and liquid phases and should be implemented in the performance analysis where phase changes are present. [6]

Chapter 3

3. Test Preparation

3.1 Test Standards

Different applicable performance test codes are available as a guide when testing a centrifugal compressor. The American Society of Mechanical Engineers (ASME) and the International Organization for Standardization (ISO) have issued specifications covering calculation methods, instrumentation, site preparation and the reporting of test results.

Testing of the impeller rig at the test facility at NTNU is conducted in accordance with ASME PTC 10, "Performance Test Code on Compressors and Exhausters". ASME PTC 10 provides specific guidelines for correct installation and location of different measuring devices and includes requirements and recommendations for performance calculation procedures. The compressor testing is conducted with the specified gas at or very near the specified operating conditions, and is classified as "Type 1" test according to ASME PTC 10.

ASME PTC 10 is based on single-phase compression. Additional measurement uncertainties must be accounted for when utilizing this code under wet gas conditions to achieve valid and accurate test results.

3.2 Test Parameters

The compressor measurement requirements are:

- Inlet pressure
- Inlet temperature
- Discharge pressure
- Discharge temperature
- Compressor flow
- Speed, torque and power

Temperature and Pressure Measurements

To evaluate thermodynamic performance, total temperature and pressure must be determined at the inlet and discharge of the compressor. [1] Total pressure is the sum of static and velocity pressure as shown in equation (3.1).

$$p = p_{static} + 0.5\rho V^2 \tag{3.1}$$

The second term in equation (3.1) will diminish at low flow rates and may be neglected in performance calculations.

Total temperature is the sum of static temperature and velocity temperature. The actual temperature measured by a sensing element is normally a value between static and total temperature depending on the ability of the sensor to recover the converted kinetic energy of the gas stream.

Total and static values for pressure and temperature are assumed to be equal if inlet and outlet compressor Mach numbers are less than 0.1. [9] For the actual compressor test, static measurements are utilized due to a low volumetric flow rate and hence low flow velocity involved.

Flow Measurement

Properly sized orifice meters are suitable for testing centrifugal compressors over a normal operating range from surge to choke. The required beta ratio of the device depends on the maximum flow rate to be measured and the range of the differential pressure transducer available.

The mass flow rate is related to the differential pressure measured over the orifice and can be determined by equation (3.2), where D is the diameter of the orifice. The equation assumes a steady flow with fully developed turbulent velocity profile through the orifice. The volumetric flow rate ($Q=m/\rho$) can then be determined, where ρ is the fluid density at the temperature and pressure measured at the orifice.

$$m = \frac{C}{\sqrt{1-\beta^4}} \varepsilon \frac{\pi}{4} D^2 \sqrt{2 \triangle p \rho_1} \tag{3.2}$$

The expansibility factor ε and the discharge coefficient C are empirically determined correction factors. The discharge coefficient relates the actual flow rate to the theoretical flow rate through the flow-measuring device. The expansibility factor takes into account

the compressibility of the fluid being monitored. Both correction factors can be determined from tables in different applicable standards or from empirical equations.

The discharge coefficient and the expansibility factor utilized for the compressor test are verified for the actual impeller rig and expected test conditions, as shown in Appendix B.

Torque, Speed and Power

Torque, speed and power are the defining mechanical variables associated with the functional performance of rotating machinery. The power output of a compressor ($P=\tau\omega$) can be determined directly from torque measurements and/or thermodynamically from the polytropic analysis shown in chapter 2.1, equation (2.5).

3.3 Test Stability

Compressor performance tests should be performed during steady state conditions. [4] The compressor and the test equipment must be operated for sufficient time at the specified operating conditions to demonstrate acceptable mechanical operation and stable values of all measurements to be taken during the compressor testing.

Steady state is achieved if the compressor measurements listed in Table 3.1 apply during a 10-minute interval. [9]

Table 3.1: Stability of compressor test [9]

Test Reading	Maximum Allowable Variation During 10-min Interval
Inlet Pressure	± 1% of Average Value
Outlet Pressure	± 1% of Average Value
Inlet Temperature	± 1°C
Outlet Temperature	± 1°C
Compressor Speed	± 10 rpm
Compressor Flow	± 1% of Average Value

Temperature measurements are especially sensitive to operational fluctuations during the compressor test. In order to reach thermal equilibrium and measure accurate temperatures, the compressor system needs sufficient time after any change in the operating conditions.

3.4 Test Points

A minimum of three readings is taken during each test interval to set up a test point. The readings are summed, and divided by the total number of readings to obtain an average. This average is utilized as the test point data.

ASME PTC 10 allows some fluctuation in a test point. The fluctuation is defined as the percent difference between the minimum and maximum test reading divided by the average of all readings and can be calculated from equation (3.3), where n is the total number of readings.

$$\text{fluctuation (\%)} = \frac{100\left(\text{highest reading - lowest reading}\right)}{\dfrac{1}{n}\displaystyle\sum_{i=1}^{n} i^{\text{th}}\,\text{reading}} \tag{3.3}$$

The permissible fluctuations of the measured parameters during a test interval are listed in Table 3.2.

Table 3.2: Permissible fluctuations of test readings [11]

Measurement	Symbol	Units	Fluctuation
Inlet Pressure	p_1	[Pa]	2 %
Inlet Temperature	T_1	[K]	0.5 %
Discharge Pressure	p_2	[Pa]	2 %
Discharge Temperature	T_2	[K]	0.5 %
Molecular Weight	M_w	[kg/kmol]	0.25 %
Speed	N	[rpm]	0.5 %
Torque	τ	[N*m]	1 %

For the measurement of inlet and discharge pressure and temperature, an average of the four independent sensors is calculated. If one recorded observation is inconsistent due to measurement error, its value should be discarded and the value determined from the average of the other three. [1]

3.5 Test Uncertainty

Test uncertainty is defined as an estimate of the limit of error of a test result. [10] Test uncertainty must be calculated to determine the accuracy of the compressor test and to validate the quality of the compressor test results.

Test uncertainty does not refer to the accuracy of a single instrument, but evaluates the complete range of possible test results given a singular test condition. Data point recorded during the test should be evaluated individually and redundant calculations should be performed to check test measurements. A sufficient number of observations will reduce the random component of uncertainty to an acceptable level.

Classification

Uncertainty sources and errors may be classified by the presumed effect on the measurement or test results. ASME PTC 19.1 [11] utilizes this classification.

Systematic error refers to an error source whose effect is constant or systematic during the test. Systematic uncertainty describes the expected limits to a systematic error. The error due to a random fluctuation of the measured quantity is referred to as *random error*. Random uncertainty refers to the expected limit of the scatter of test data. By recording more measurements of the test quantity this error can be reduced.

The time interval and duration of the test must be clearly specified for classifying an error as either random or systematic. The *total error* in a measurement is the combination of systematic and random errors. The difference between the true and the measured value is the total error, as shown in Figure 3.1.

Systematic and random uncertainties are both defined at the standard-deviation level as "standard uncertainties". An uncertainty level of 95% is commonly used in ASME PTC 19.1.
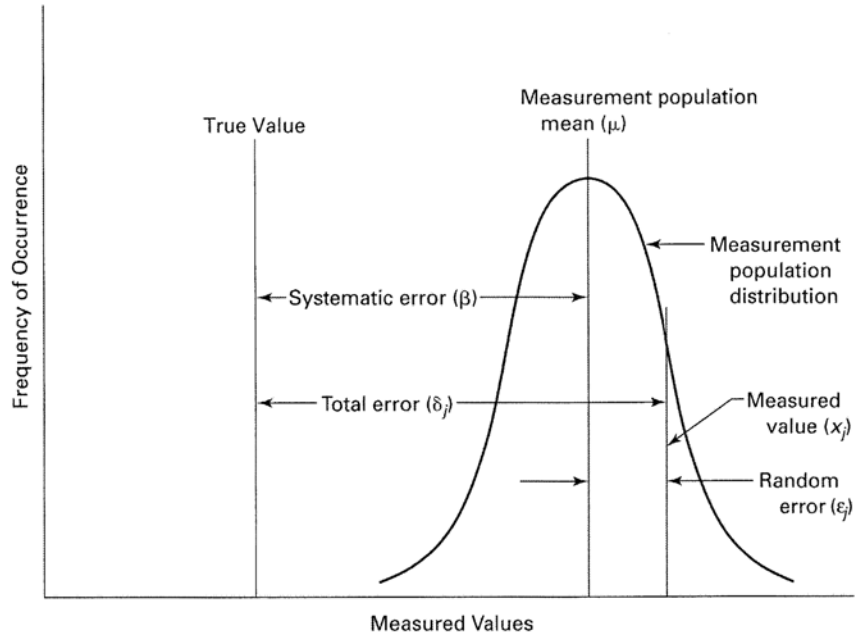
Figure 3.1: Illustration of measurement errors [11]

Measurement uncertainty

Deviations in the ideal or recommended test conditions and procedures will increase the individual measurement uncertainties. This can result in a higher total uncertainty for the centrifugal compressor. The uncertainty in the pressure or temperature measurements may result from disturbances in the flow field upstream or downstream the compressor. Installation requirement in ASME PTC 10 ensures that these uncertainties are minimized or negligible by taking sufficient observation to ensure that the average measurements will be accurate.

If piping vibration or flow-induced pulsations are high at the location of the static pressure measurement, the measurement of pressure will show a significantly higher random uncertainty. Wall conduction heat transfer to and from temperature sensor contributes to the temperature measurements error.

Calibration

Proper calibration of the instruments can reduce the measurement uncertainty. All pressure measurements are referred to devices that serve as primary standards of pressure measurements. A big contribution to the uncertainty of pressure measurements is the errors accumulated in the propagation of the measurement uncertainty along a calibration chain and not from the primary standard. [12]

16

Data acquisition

Error in the data acquisition system contributes to the overall uncertainty. Calibration of the overall system can minimize this effect.

Data reduction uncertainty

Care must be taken when averaging data. Averaging on raw test data may cause unacceptable deviations and should be avoided. The computational uncertainty is commonly assumed negligible due to advanced computer systems.

Chapter 4

4. Compressor Test Facility

4.1 Impeller Rig

The values given for the impeller rig are the values at design point. Some discrepancies between design point and actual operating point are expected.

The test compressor is composed of an impeller proceeded by a vaneless radial diffuser and a volute as shown in Figure 4.1.
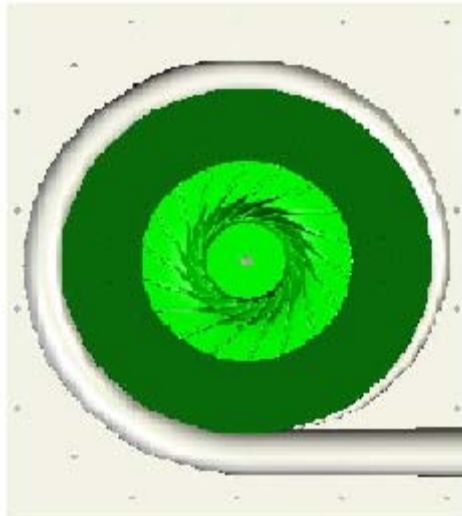
Figure 4.1: Test compressor

The shrouded test impeller shown in Figure 4.2 contains 18 blades with a back sweep of 50° at the exit. Splitter vanes can be implemented by removing sections of the existing impeller blades. At design point flow rate of 1.0 m^3/s, a work input coefficient of 0.69 is assumed so that the impeller would have enough pressure-rise to produce a stage pressure ratio of 1.39 and polytropic efficiency of 80%. The compressor design speed is 10 000 rpm. The frequency of the impeller rotation is 166.78 Hz, with a blade passing frequency of 3002.04 Hz, half that for potential splitter vanes.
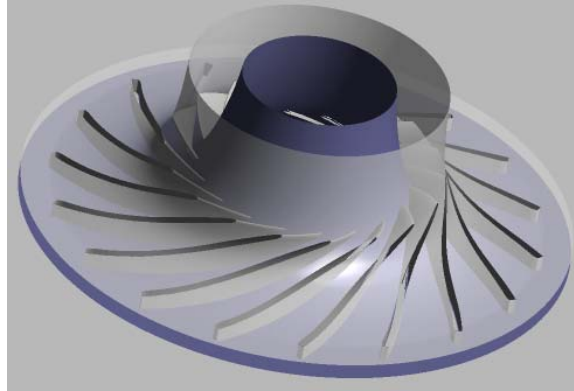
Figure 4.2: Test impeller

Atmospheric air is drawn into the compressor through an orifice plate located in the suction pipe. When testing the compressor for wet gas conditions liquid can be sprayed into the gas flow from an injection-module placed downstream of the orifice to assure correct flow measurements.

A high-speed motor drives the compressor with a frequency converter for speed control. The desired pressure ratio is reached by means of a butterfly valve. The throttling valve is mounted to a divergent pipe segment installed at the discharge pipe due to dissimilar diameters at pipe and valve. Adjusting the exit area of the valve with a rotary actuator controls the compressor mass flow. After passing through the throttle valve, the air is exhausted to the atmosphere. The test rig is shown in Figure 4.3.

Figure 4.3: NTNU test rig

4.2 Piping Configuration

Figure 4.4 shows the pipe length recommendation upstream the compressor according to ASME PTC 10 [1] and ISO 5167 [13].

The orifice with beta value 0.64 requires a straight pipe length of 5.0m (20D) upstream and 0.875m (3.5D) downstream the device to assure a correct flow reading. The requirement of straight pipe length given by the vendor of the orifice is in accordance with the ISO 5167 recommendations for a single bend pipe. If an orifice with lower beta value is chosen, shorter pipe lengths are required owing to the lower pressure drop over the device.

The compressor has an axial inlet that may produce a vortex at the pressure station under various conditions. The static pressure stations at the inlet are installed at a minimum of 1.0m (4D) upstream the compressor flange to avoid errors in the measurement of inlet pressure.
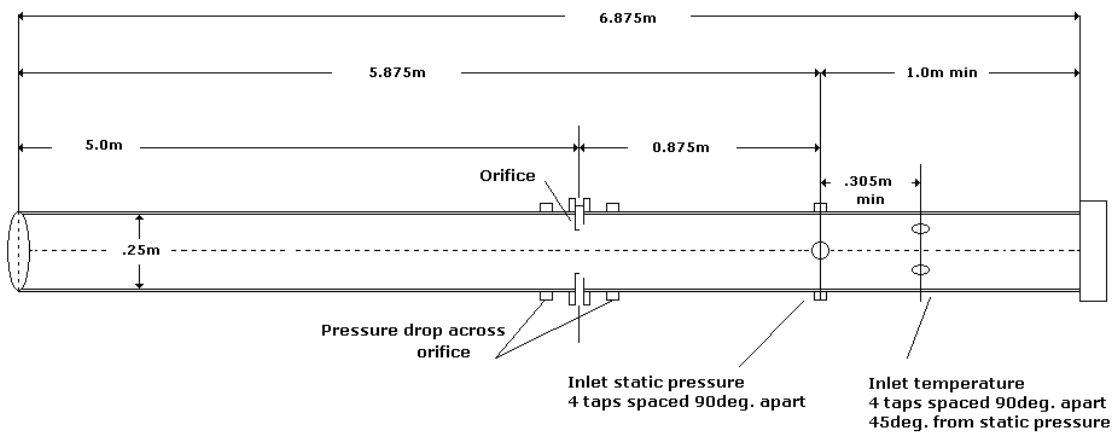
Figure 4.4: Inlet piping and instrumentation

The static pressure stations at the discharge are installed 0.6618m (6D) from the compressor exit due to the un-symmetrical flow produced by the compressor volute.
Figure 4.5 shows the ASME PTC 10 pipe length recommendation downstream the compressor.
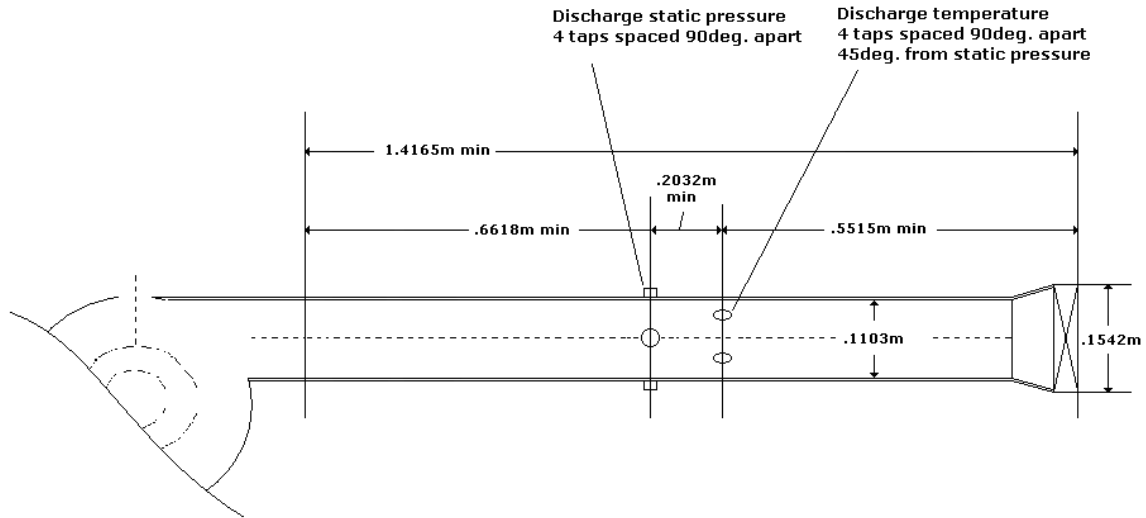
Figure 4.5: Discharge piping and instrumentation

4.3 Apparatus and Instrumentation

Table 4.1 shows an overview of the instrumentation utilized for the impeller test rig.

Table 4.1: Impeller test rig – instrumentation list

	Element Type	Number
Pressure	Pressure Transmitter, APCE-2000	8
Temperature	Pt 100 (IEC 751)	8
Flow	Orifice: Plate-Standard, Corner (Beta value 0,6401)	1
	Orifice: Plate-Standard, Corner (Beta value 0,4018)	1
Torque Transducer	HBM T-12 Digital torque transducer, with BSD-MODULFLEX Coupling system	1

Pressure Instrumentation

Four pressure measurements are taken at the inlet and discharge piping of the compressor. Figure 4.6 shows the pressure transmitter utilized for the measurements. The pressure transmitters work by converting changes in the resistance of a piezoresistance silicon sensor, which are proportional to the pressure difference being measured, into a standard current signal. The uncertainty of the pressure transmitter is 0.1%.

Figure 4.6: APCE-2000 pressure transmitter

Temperature Instrumentation

Four temperature measurements are taken at the inlet and discharge piping of the compressor by resistance temperature devices. Figure 4.7 shows the Pt 100 element utilized for the temperature measurements. The sensors measure the changes in resistance of a platinum wire that is coiled together to form a ceramic core. The changes in resistance are converted to a standard voltage signal. Pt 100 elements are assumed to be highly accurate with great temperature sensitivity. The uncertainty of the pressure transmitter is 0.05%.
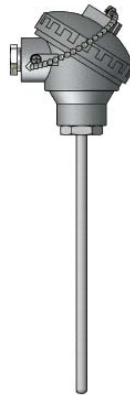
Figure 4.7: Pt 100 sensor

Figure 4.8 shows the pressure and temperature sensors located at compressor inlet, while Figure 4.9 shows the sensors at outlet.
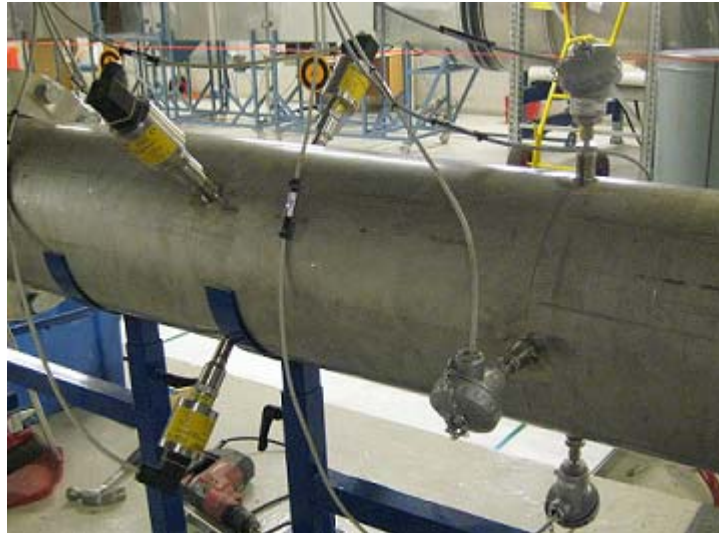
Figure 4.8: Pressure and temperature sensors at inlet

Figure 4.9: Pressure and temperature sensors at outlet

Flow Instrumentation

An orifice with beta value 0.64 located at the inlet piping measures the flow through the compressor. Two static pressure taps located on opposite sides of the orifice measure the differential pressure over the orifice. An orifice with beta value 0.40 for measuring smaller fluid flows can replace the orifice.

Orifice meters with beta ratios less than 0.65 have a flow measurement uncertainty of less than 1.5%. [9] The orifice accuracy will not be influenced by liquid present due to the downstream location of the injection module. Hence a multiphase correction of the device is not required.

Torque, Speed and Power Instrumentation

Torque, rotational speed and power are determined by utilizing a digital measurement system. The torque transducer is connected to the shaft through a torque-sensing coupling. The torque transducer provides a digital signal proportional to the measured torque. Figure 4.10 and Figure 4.11 shows respectively the digital torque transducer and the coupling system.

Figure 4.10: HBM T-12 digital torque transducer
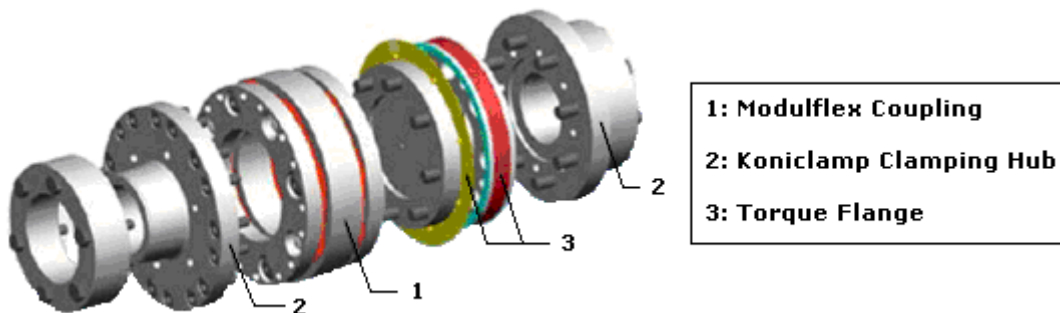
Figure 4.11: BSD-MODULFLEX coupling system

Instrumentation for Instability Measurements

Pressure fluctuations caused by instabilities and the resulting vibration of the rotor can be measured with variation of flow rate and impeller rotating speed to document and determine the cause of the instability phenomenon.

Due to late delivery of the compressor components, the sensors for instability measurements are not yet implemented in the compressor rig. The recommended measurement procedures, instrumentation and location of sensors are described in chapter 7.4-7.7. Multiphase flow measurement and visualization techniques and instrumentation are described in chapter 8.

4.4 Data Acquisition System

Automatic parameter registration is performed with "Lab View"-software on a digital computer. The computer monitors all measured parameters by transforming the analog signals from the pressure transmitters and temperature sensors into digital data. The performance equations can be implemented directly into Lab View.

Chapter 5

5. Compressor Test

The construction of the compressor rig was behind time due to late deliveries of the compressor components and instrumentation. The performance calculations are based upon one compressor test conducted with dry gas at part-load. The results are utilized to validate the compressor behavior at the test operating condition.

Instrumentation for detection of compressor instabilities is not yet implemented in the compressor test rig. Documentation of compressor instability is therefore discarded. Recommended methods, procedures and instrumentation for wet gas is instead presented in chapter7.4-7.7. Visualization techniques are presented in chapter 8.

5.1 Test Matrix

The compressor test is conducted at part load, with 5000 rpm. By gradually adjusting the butterfly valve, the compressor mass flow is controlled. Lab View registers the test parameters with a logging frequency of approximately three second. Table 5.1 shows the intended test matrix consisting of ten test points at rotational speed of 5000 rpm.

Table 5.1: Initial test matrix at part load

	Speed, N	Flow, Q_1
	[rpm]	[m^3/s]
1	5000	0,40
2	5000	0,45
3	5000	0,50
4	5000	0,55
5	5000	0,60
6	5000	0,65
7	5000	0,70
8	5000	0,75
9	5000	0,80
10	5000	0,85

5.2 Performance Procedure

The compressor rig at the NTNU test facility is tested at atmospheric inlet conditions with a design stage pressure ratio of 1.39. In cases where the pressure is small relative to the critical pressure ($p_c=37,7bar$) and/or the temperature is large relative to the critical temperature ($T_c=133K$), a near ideal gas behavior may be assumed. [14] At such conditions the ideal polytropic procedure can be utilized to determine the compressor performance. Assumptions made in advance for the compression gas and performance procedures must always be verified for the actual test and operating range.

In compression cases where the Schultz polytropic exponent is approximately equal to the ideal polytropic exponent and the Schultz correction factor is one, the two polytropic procedures give equivalent results, as shown in Appendix A.3. The ideal polytropic procedure is, in such cases, often preferred in reference to the Schultz procedure because of the simplicity of the ideal polytropic calculations. The polytropic procedure is, for this particular test, preferred because the polytropic calculation procedures are more easily implemented in the Lab View software.

PRO/II Simulation

The sensitivity and validity of the performance calculations are evaluated by implementation of the compression routines in the process simulation system PRO/II. PRO/II has implemented the Schultz polytropic procedure for performance calculations. The PRO/II simulation setup is shown in Appendix C. By varying the compressor operating conditions, the sensitivity of the calculation procedures is identified and the procedures validated for the actual compressor test and operating range.

PRO/II utilizes the mass flow, outlet temperature and pressure to estimate the specific outlet volume from an appropriate EOS, and hence to determine the polytropic exponent. The PRO/II calculations are congruent with the calculation procedures given in the ISO and ASME standards for cases with *known* outlet conditions. For cases with *unknown* outlet conditions PRO/II utilizes iterative processes for the performance calculations.

Comparison of Ideal Polytropic and Schultz Polytropic Procedures

Schultz compressibility functions, *X* and *Y*, approach respectively zero and one for the gas inlet condition, as shown by the generalized compressibility charts given in Appendix D. Schultz polytropic exponent will thus approach the ideal polytropic exponent.

To verify the assumption of ideal gas behavior for the compressor test, the compressibility factor, *Z*, is set equal to 1 to determine the specific volumes and hence the ideal polytropic exponents from the equations given in chapter 2.1 and Appendix A.1. The polytropic exponent is in addition determined from simulations in PRO/II for

comparison, since PRO/II gives a polytropic exponent corresponding to the Schultz polytropic exponent.

The accuracy of the thermodynamic properties calculated by PRO/II depends on the validity of the selected EOS for the specified gas and thermodynamic condition. The BWRS equation is utilized for the performance simulations. The BWRS equation of state is found to give approximately equal values to the ideal equation of state by simulations in PRO/II for the compressor operating range.

Table 5.2 and Table 5.3 show representative measured parameters for the compressor test and calculated performance data at compressor inlet and discharge with the assumption of ideal gas behavior.

Table 5.2: Measured and calculated test parameters at inlet with $Z=1$

p_1	T_1	Q_1	ρ_1	v_1	m
[bar]	[K]	[m^3/s]	[kg/m^3]	[m^3/kg]	[kg/s]
0,937	296,20	0,83	1,10	0,91	0,92
0,941	296,53	0,81	1,11	0,90	0,89
0,949	296,64	0,77	1,12	0,90	0,85
0,973	296,65	0,60	1,14	0,88	0,68
0,978	296,72	0,54	1,15	0,87	0,62
0,983	296,72	0,49	1,15	0,87	0,56
0,990	296,71	0,41	1,16	0,86	0,48

Table 5.3: Measured and calculated test parameters at discharge with $Z=1$

p_2	T_2	Q_2	ρ_2	v_2	m
[bar]	[K]	[m^3/s]	[kg/m^3]	[m^3/kg]	[kg/s]
0,999	302,88	0,80	1,15	0,87	0,92
1,007	303,43	0,77	1,16	0,86	0,89
1,023	303,82	0,73	1,17	0,85	0,85
1,065	304,20	0,56	1,22	0,82	0,68
1,074	304,46	0,51	1,23	0,81	0,62
1,082	304,50	0,45	1,24	0,81	0,56
1,091	304,63	0,38	1,25	0,80	0,48

Table 5.4 shows a direct comparison between the corresponding calculated ideal polytropic exponent and the estimated Schultz polytropic exponent given by PRO/II. The corresponding values for the polytropic head are given in Table 5.5.

Table 5.4: Comparison of the polytropic exponent

n at Z=1	n_v - PRO/II	Deviation	Relative Deviation [%]
1,5662	1,5674	0,0012	0,0766
1,4712	1,4720	0,0008	0,0543
1,5091	1,5101	0,0010	0,0662
1,3989	1,3995	0,0006	0,0429
1,4191	1,4198	0,0007	0,0493
1,3644	1,3648	0,0004	0,0293
1,3757	1,3762	0,0005	0,0363

Table 5.5: Comparison of the polytropic head

H_p [J/kg] n at Z=1	$H_{p,S}$ [J/kg] n_v - PRO/II	Deviation [J/kg]	Relative Deviation [%]
5507,35	5507,44	0,0865	0,0016
5859,15	5859,22	0,0740	0,0013
6434,15	6434,26	0,1058	0,0016
7774,37	7774,48	0,1079	0,0014
8051,74	8051,87	0,1310	0,0016
8254,13	8254,21	0,0852	0,0010
8415,02	8415,13	0,1088	0,0013

The Schultz polytropic exponent given by PRO/II has a maximum deviation of 0.0766% from the calculated ideal polytropic exponent. The corresponding deviation for the Schultz polytropic head is 0.0016%.

The values estimated by PRO/II agree closely with the calculated values determined by the ideal gas equations and thus verify the use of ideal polytropic calculation procedures for the compressor test.

The validation of the ideal polytropic procedure will only be accurate for the specified gas and test condition. For higher pressure and temperatures, the Schultz polytropic procedure must be implemented and verified for the real gas behavior.

Sensitivity of Polytropic Head

Deviation between ideal and Schultz polytropic exponents will for low pressure ratios only slightly influence the calculation of polytropic head, and can in such cases be neglected. For higher pressure ratios, similar deviation may strongly influence the polytropic head and must be accounted for. Table 5.6 shows how deviation between the polytropic exponents will influence the deviation in polytropic head for different pressure ratios.

Table 5.6: Deviation between the polytropic exponents for various pressure ratios

$p_2/p_1 = 1{,}09$		$p_2/p_1 = 1{,}39$ (Design)		$p_2/p_1 = 10$	
n	H_p	n	H_p	n	H_p
Relative deviation [%]		Relative deviation [%]		Relative deviation [%]	
3,24	0,10	0,84	0,10	0,11	0,10
16,21	0,50	4,19	0,50	0,55	0,50
32,47	1,00	8,40	1,00	1,10	1,00
65,16	2,00	16,86	2,00	2,21	2,00

If the polytropic exponents deviate with 3.24%, the polytropic heads will deviate with 0.1% for a pressure ratio of 1.09. To be within the same deviation in head, the polytropic exponents can only deviate with 0.84% and 0.11% for pressure ratios of respectively 1.39 and 10. This verifies that the sensitivity of the ideal polytropic head calculation is notably low in the compressor operating range, but will be substantially higher for greater pressure ratios. The Schultz polytropic analysis must then be implemented to achieve accurate performance results.

Isentropic Exponent

The Schultz polytropic analysis utilizes the isentropic reference process in predicting the correction factor, f, and hence the polytropic head. Variation in isentropic exponent may therefore strongly influence the calculated polytropic head. PRO/II simulations show that the Schultz correction factor, f, is constant and equal to one in the compressor operating range, and is not influenced by variation in isentropic exponent.

Table 5.7 shows that variation in the isentropic exponent estimated by PRO/II are small with varying pressure ratio and can be neglected for performance calculations in the compressor operating range.

Table 5.7: Variation in isentropic exponent with varying pressure ratio

p_2/p_1	K
[-]	[-]
1,002	1,4027
1,010	1,4031
1,050	1,4031
1,090	1,4031
1,500	1,4030
2,000	1,4028

Sensitivity of Polytropic Efficiency

Variations in polytropic exponent, with approximately constant isentropic exponent, will highly influence the calculated polytropic efficiency, as seen in Table 5.8

Table 5.8: Variation in polytropic efficiency with varying polytropic exponent

n	κ	η_p
[-]	[-]	[-]
1,9187	1,4031	0,60
1,7921	1,4031	0,65
1,6961	1,4031	0,70
1,6209	1,4031	0,75
1,5603	1,4031	0,80
1,5106	1,4031	0,85
1,4689	1,4031	0,90
1,4335	1,4031	0,95
1,4031	1,4031	1,00

Table 5.9 shows the sensitivity of the polytropic efficiency with deviation in polytropic exponents from the first three test points in Table 5.4.

Table 5.9: Sensitivity of polytropic efficiency with varying polytropic exponent

η_p [-]	$\eta_{p,s}$ [-]	Deviation	Relative Deviation
n at Z=1	n_v - PRO/II	[-]	[%]
0,7947	0,7936	0,0011	0,1352
0,8970	0,8960	0,0010	0,1153
0,8516	0,8505	0,0011	0,1301

The larger difference between the calculated ideal polytropic exponent for the compressor test and the Schultz exponent estimated from PRO/II is 0.0012, a relative deviation of 0.0766%. As shown in Table 5.5, the polytropic head then holds a relative deviation of 0.0016%. In comparison, the calculated polytropic efficiency will have a relative deviation of 0.1352% at constant isentropic exponent ($\kappa=1.4031$). Hence the polytropic efficiency is more sensitive for deviations in polytropic exponent than the polytropic head.

The polytropic efficiency calculated for the compressor test turned out to be extremely high, indicating that one or more parameters are measured inaccurately or that the presumed constant isentropic exponent is incorrect. Chapter 6 shows the effect of measurement uncertainties on the performance calculations for a case representative to the compressor test. Due to the low pressures involved for the actual compressor test, the polytropic head and efficiency are highly sensitive to uncertainties in the pressure measurements. Uncertainties in temperature measurements will only slightly influence the polytropic head, but will have strong influence on the polytropic efficiency.

EOS Sensitivity

The selected EOS for the performance simulations in PRO/II is the BWRS equation. Since the calculated performance may vary depending on the implemented EOS, a sensitivity analysis is conducted.

The polytropic head deviations for the various equation of state compared to the calculated ideal equation are given in Table 5.10. The operating condition and calculated parameters for ideal gas behavior are shown in Table 5.11.

Table 5.10: Variation in polytropic head with different equation of state

PRO/II	n	H_p	Rel. Deviation, H_p
	[-]	[J/kg]	[%]
Ideal	1,5662	5507,35	0,0000
BWRS	1,5674	5507,44	0,0016
SRK	1,5679	5507,47	0,0022
PR	1,5675	5507,44	0,0017

Table 5.11: Operating data for compressor test

p_1	[bar]	0,94
T_1	[K]	296
p_2	[bar]	1,00
T_2	[K]	303
κ	[-]	1,4031
n	[-]	1,5662
η_p	[-]	0,79
H_p	[J/kg]	5507

Table 5.10 demonstrates that deviations in the polytropic head with different EOS are negligible for the actual compressor performance evaluation. The BWRS equation of state gives a polytropic head with a relative deviation of 0.0016% to the ideal equation. The different EOS yield similar results for the polytropic head within an accuracy range of 0.0017%-0.0022%.

The negligible values for relative deviation with different EOS verifies that at states where the pressure is small relative to the critical pressure, the ideal EOS will provide a suitable approximation. For higher pressures and real gases, the ideal EOS is not valid. The selected EOS must always be verified for the actual compressor operating range and fluid composition.

5.3 Generation of Performance Curves from Recorded Data Points

The compressor behavior referred to constant operating conditions and constant compressor geometry is presented in the form of performance curves.

Dimensional analysis techniques are often conducted in order to eliminate the excessive number of experiments required to obtain a complete presentation of the variables over the expected operating range. Since the NTNU impeller rig is operated at approximately constant atmospheric inlet conditions with stable air properties, a dimensional analysis is not necessary. Curves of delivery pressure and polytropic head are plotted against volumetric flow for various fixed values of speed are utilized to generate the performance curves.

Test Point

The compressor test points are each determined from three test readings registered by Lab View for the calculation of average test values. The fluctuations for each test parameter in the test points are calculated in accordance with ASME standard procedures. Test points with fluctuations outside the limits given by ASME PTC 10 are discarded. The valid test point is shown in Appendix E.

Table 5.12 displays the measured parameters together with the calculated pressure ratio and polytropic head for six representative test points. The corresponding polytropic head curve is shown in Figure 5.1. The pressure ratio with varying volume flow is shown in Figure 5.2.

Table 5.12: Measured test parameters and calculated test results

Test Point	Measured						Calculated	
	p_1	T_1	Q_1	p_2	T_2	N	p_2/p_1	H_p
	[bar]	[K]	[m³/s]	[bar]	[C]	[rpm]	[-]	[J/kg]
11	0,94	296,2	0,83	1,00	302,9	4983	1,07	5505
25	0,94	296,5	0,81	1,01	303,4	4951	1,07	5863
35	0,95	296,6	0,77	1,02	303,8	4937	1,08	6430
44	0,97	296,6	0,60	1,06	304,2	4948	1,09	7772
55	0,98	296,7	0,54	1,07	304,5	4951	1,10	8045
60	0,99	296,7	0,41	1,09	304,6	4966	1,10	8447
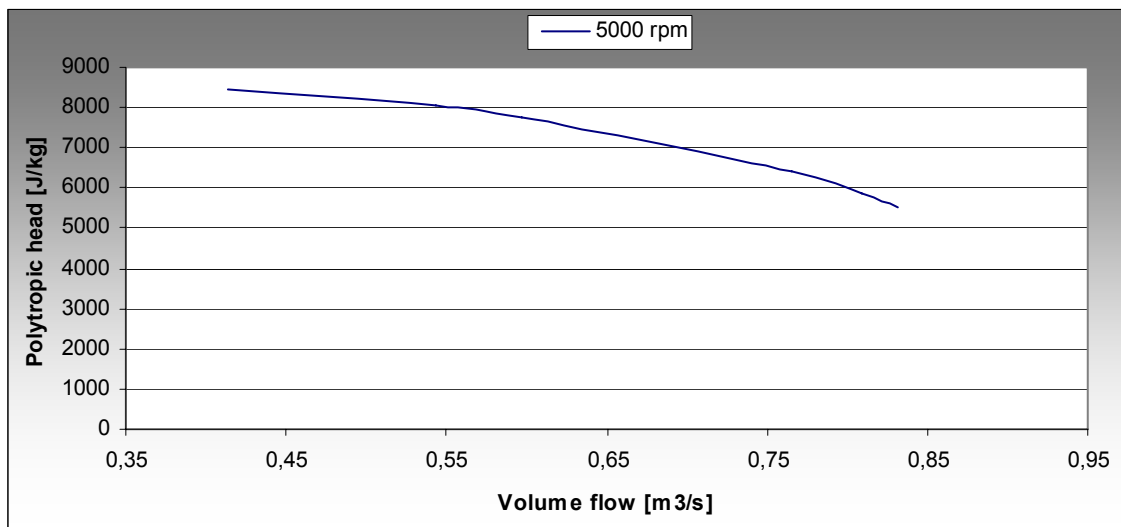
Figure 5.1: Polytropic head curve
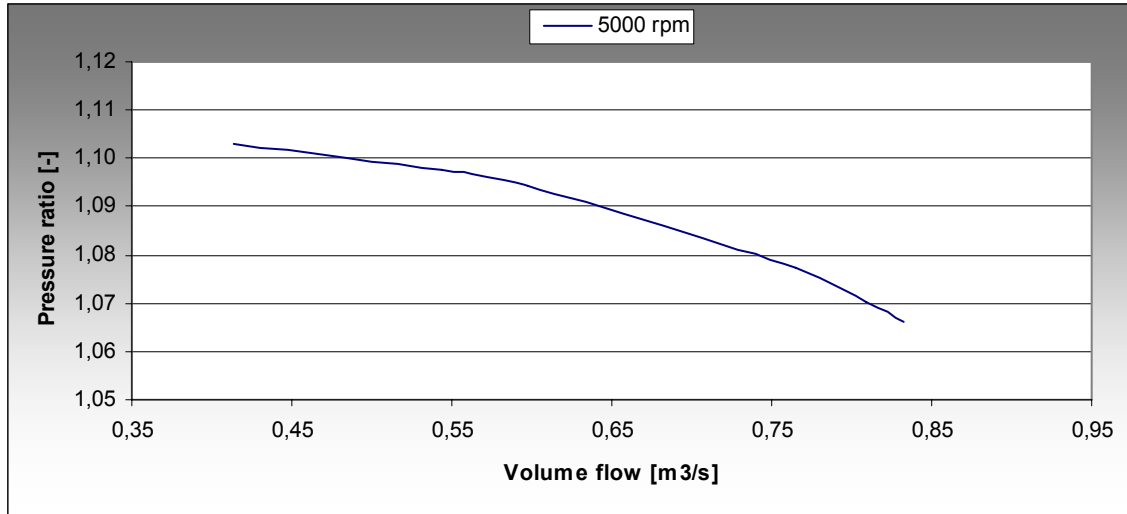
Figure 5.2: Pressure ratio with varying volume flow

Non-dimensional head and flow coefficients

The average of the data point at a particular operating condition is used to calculate the average head and flow coefficients. The non-dimensional head and flow coefficients describe the aerodynamic and mechanical performance of a centrifugal compressor and are used to adjust for differences in test conditions in order to match the flow characteristics when the compressor is tested under varying conditions.

The polytropic head coefficient is given in equation (5.1). The tangential velocity ($U=\pi DN/60$) is calculated at the impeller exit diameter (0.385m). The flow coefficient is given in equation (5.2).

$$\psi_p = \frac{H_p}{U^2} \tag{5.1}$$

$$\varphi = \frac{Q_1}{2\pi \dfrac{N}{60} D^3} \tag{5.2}$$

Figure 5.3 shows the head versus flow coefficient curve for the compressor test at approximately 5000 rpm. The calculated values for the polytropic head coefficient and flow coefficient are given in Appendix F.
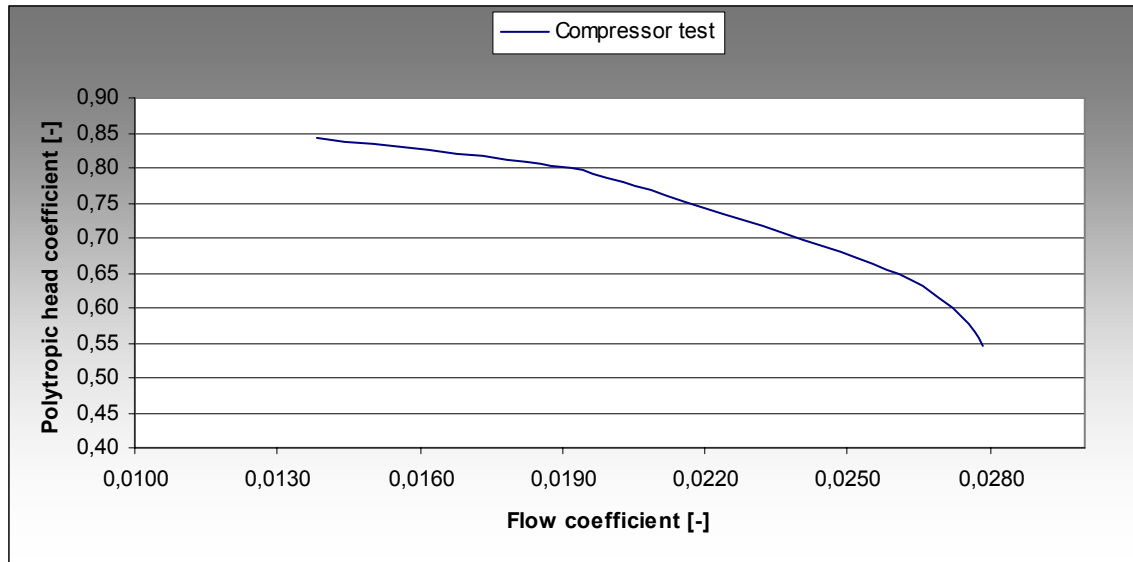
Figure 5.3: Polytropic head versus flow coefficient performance curve

5.4 Affinity Laws

To predict the compressor performance at different rotational speeds, the affinity laws, equation (5.3) and equation (5.4), are utilized.

$$H = H_{ref} \left(\frac{N}{N_{ref}} \right)^2 \qquad (5.3)$$

$$Q = Q_{ref} \left(\frac{N}{N_{ref}} \right) \qquad (5.4)$$

The affinity laws allow prediction of the head discharge characteristic of a compressor from a known characteristic measured at a different speed or impeller diameter. The affinity laws are applicable only if the compressor flow is kinematic and dynamic similar. Kinematic similarity yields when the velocity diagrams are similar for the different flow conditions. Dynamic similarity is achieved when the corresponding reduced velocities are of the same size. The efficiency is held constant in the deduction of the laws.

Table 5.13 shows the calculated volume flow and polytropic head for rotational speed 7000 rpm and 10 000 rpm. A comparison of the polytropic head curves is shown in Figure 5.4.

Table 5.13: Predicted performance given by the affinity laws

Test Point	5000 rpm		7000 rpm		10 000 rpm	
	Q_1	H_p	Q_1	H_p	Q_1	H_p
	[m³/s]	[J/kg]	[m³/s]	[J/kg]	[m³/s]	[J/kg]
11	0,83	5505	1,16	7707	1,66	11010
25	0,81	5863	1,13	8208	1,62	11725
35	0,77	6430	1,07	9002	1,53	12860
44	0,60	7772	0,84	10881	1,19	15544
55	0,54	8045	0,76	11262	1,09	16089
60	0,41	8447	0,58	11826	0,83	16894
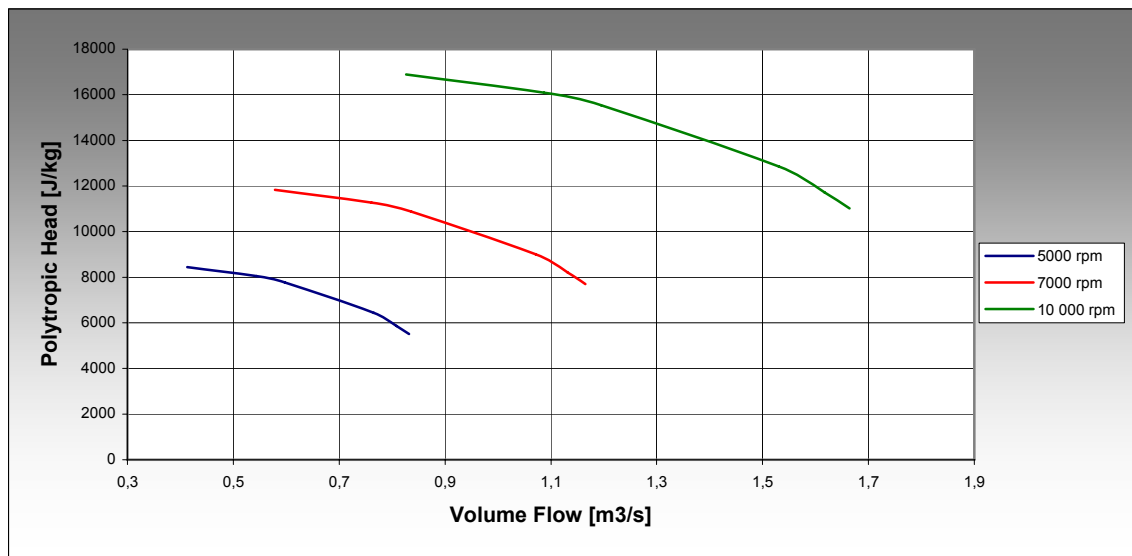
Figure 5.4: Polytropic head curves given by the affinity laws

5.5 Test Stability

Table 5.14 shows the deviations in test parameters compared to the average values of the test points. The measured parameters are outside the limits given by ASME PTC 10, Table 3.1.

Due to the low pressures involved for the compressor test, the measurements of pressure are highly sensitive to fluctuations. Fluctuations in test condition, with regard to temperature, are most likely caused by the temperature rise in the test facility. As described in chapter 3.3, the compressor needs sufficient time after any change in operating condition to reach thermal equilibrium and hence measure accurate temperatures. The fluctuating speed may be the result of an unstable compressor shaft or uncertainties in the frequency converter.

Table 5.14: Test stability

Test Parameter	SI Unit	Average Value	Highest	Lowest	Deviation	Allowable Deviation
p_1	[bar]	0,96	0,99	0,94	5,87 %	± 1%
p_2	[bar]	1,03	1,09	1,00	9,34 %	± 1%
T_1	[K]	296,5	296,8	295,7	1,13 K	± 1K
T_2	[K]	303,6	304,6	302,2	2,38 K	± 1K
N	[rpm]	4963	5063	4877	186 rpm	± 10 rpm

5.6 Static Measurement Uncertainty

At Mach numbers < 0.1 the total and static values for pressure and temperature are assumed to be the same. [9] Table 5.15 gives the inlet and outlet Mach numbers for the compressor test points.

Table 5.15: Mach numbers at inlet and outlet

Test Point	Inlet				Outlet			
	Q_1 [m³/s]	V_1 [m/s]	a_1 [m/s]	Ma_1 [-]	Q_2 [m³/s]	V_2 [m/s]	a_2 [m/s]	Ma_2 [-]
11	0,83	17,0	345,0	0,05	0,80	85,5	348,9	0,24
25	0,81	16,5	345,2	0,05	0,77	80,9	349,2	0,23
35	0,77	15,6	345,2	0,05	0,73	76,1	349,4	0,22
44	0,60	12,2	345,2	0,04	0,56	58,6	349,6	0,17
55	0,54	11,1	345,3	0,03	0,51	53,2	349,8	0,15
60	0,41	8,4	345,3	0,02	0,38	40,3	349,8	0,12

The Mach number requirement is satisfied for the inlet measurements. The higher Mach numbers at outlet are due to a smaller outlet diameter that results in a higher velocity at the measuring station.

The velocity component of the measurements cannot be assumed negligible at the outlet measuring station. An additional uncertainty must be accounted for due to a greater difference between total and static pressure and temperature.

5.7 Wet Gas Predictions

The presence of liquid in a compression process will decrease the discharge temperature and increase the fluid discharge density due to evaporate cooling of the gas phase. [7] A change in relative volume flow through the compressor due to increased discharge density results in a change in compressor performance and efficiency as shown in respectively Figure 5.5 and Figure 5.6.
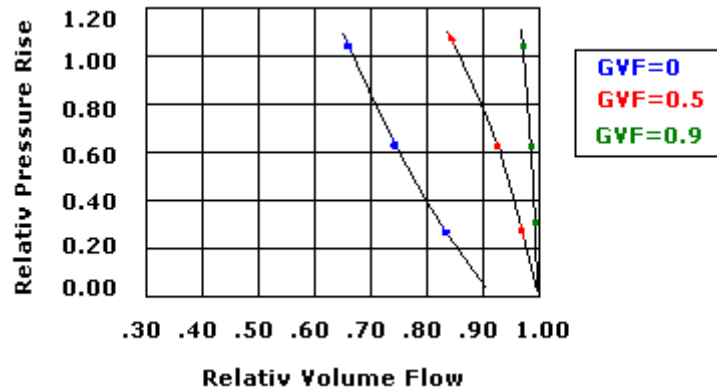
Figure 5.5: Pressure rise with different GVF [15]
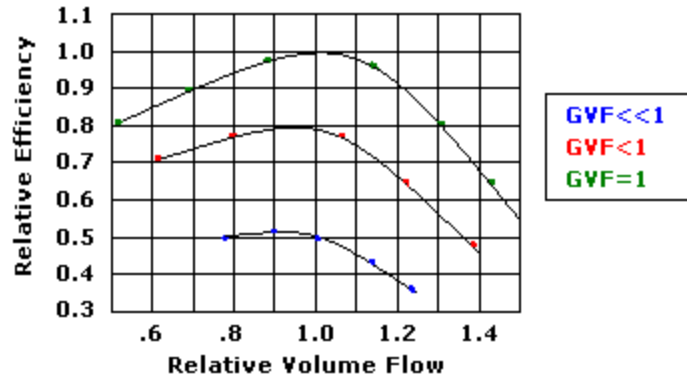
Figure 5.6: Efficiency with different GVF [15]

The gas liquid content is given by the gas volume fraction in equation (5.5).

$$GVF = \alpha = \frac{Q_g}{Q_g + Q_l} \tag{5.5}$$

Figure 5.6 indicate a more narrow operating range for the wet gas compressor, as the curves shift to left with increasing GVF. A narrow operating range will result in a reduced surge margin for the wet gas compressor. Figure 5.7 show that the efficiency for wet gas compression is expected to decrease with increasing liquid content.

The direct integration procedure, as presented in chapter 2.3, is suitable for wet gas compression and must be applied in performance analysis where phase changes along the compression path are present. Phase transitions are dependent on the fluid inlet composition and compressor operating condition.

The probability for phase changes to occur is limited for the actual compressor test due to the low compressor pressure ratio and the atmospheric inlet condition, and can thus be neglected in the performance evaluation. Performance procedures based on the polytropic assumptions will then be accurate for the actual test. Wet gas testing must be conducted to ensure the validity of this assumption for the compressor operating range.

Since phase transitions are assumed negligible, the BWRS will be an applicable EOS for the planned wet gas compressor test. At higher pressure ratios this assumption is not valid, and an EOS that takes into account any phase transitions must be utilized. The GERG EOS gives accurate density values in both vapor and liquid phases and is recommended for the wet gas analysis.

When utilizing static measurements for the wet gas performance calculations, the uncertainties will be substantially higher. The speed of sound ($a=(\kappa RT)^{1/2}$) will be severely degraded when liquid is introduced due to greater molecular weight. The Mach number ($Ma=V/a$) is inversely proportional to the speed of sound and will increase as the speed of sound decreases. Total measurements must be implemented for the performance evaluation, even for low volumetric rates.

Figure 5.7 shows how the gas volume fraction, GVF, will influence the speed of sound in a typical natural gas composition. [7]
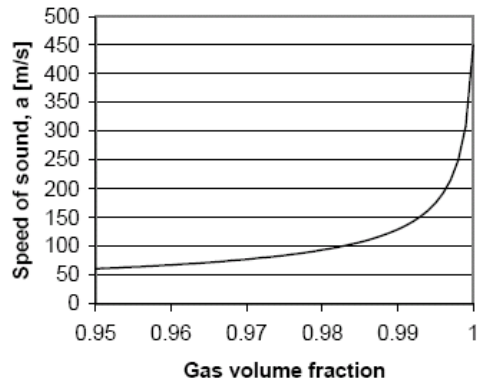
Figure 5.7: Speed of sound with different GVF [7]

5.8 Conclusion Chapter 5

The values estimated for polytropic exponent and polytropic head by PRO/II agree closely with the calculated values determined by the ideal gas equations and thus verify the use of ideal polytropic calculation procedures for the compressor test. The sensitivity of the ideal polytropic head is notably low in the compressor operating range, but will be substantially higher for greater pressure ratios. The polytropic efficiency is shown to be more sensitive for deviations in polytropic exponent than the polytropic head for the compressor test.

The thermodynamic equation of state for ambient air is verified to be consistent with the ideal gas law in the compressor pressure and temperature range. Deviations in the performance procedures with different equation of state are negligible for the actual performance evaluation. The ideal EOS provides an acceptable approximation at many states, but will be highly inaccurate at states with high pressures and temperatures.

Variations in isentropic exponent estimated by PRO/II are small with varying pressure ratio and can be neglected for performance calculations in the compressor operating range.

The probability for phase changes to occur is limited for the planned wet gas compressor test due to the low compressor pressure ratio and the atmospheric inlet composition and can thus be neglected in the performance evaluation. Performance procedures based on polytropic assumptions will be accurate for the planned wet gas compressor test.

When converting the performance results for the compressor test to real gases at high pressure and temperature conditions, the ideal assumptions will not be applicable. The Schultz polytropic analysis must be utilized to achieve accurate results. An applicable EOS for the gas condition and operating range must be implemented in the procedures.

Chapter 6

6. Measurement Sensitivity

A sensitivity analysis is conducted in order to determine the effect of measurement uncertainties on the performance calculations. By changing the test parameters one at a time deviations in polytropic head is analyzed.

The sensitivity analysis is performed for to different cases. The analysis for case 1 is conducted with outlet conditions representative for the actual compressor test. Case 2 is conducted to determine the measurement sensitivity for the performance calculations at higher outlet pressure and temperature.

6.1 Case 1

The test parameters utilized in the sensitivity analysis for case 1 are given in Table 6.1. Table 6.2 displays the constant input values for the performance calculations. The calculated values resulting from the sensitivity analysis are shown in Appendix G.1.

Table 6.1: Reference test parameters – Case 1

Test Parameters	Symbol	Reference Test Point	Units
Inlet Pressure	p_1	0,95	[bar]
Outlet Pressure	p_2	1,01	[bar]
Inlet Temperature	T_1	295	[K]
Outlet Temperature	T_2	302	[K]

Table 6.2: Test point constants

Test Parameters	Symbol	Reference Test Point	Units
Compressibility Constant	Z	1	[-]
Inlet Temperature	R	287	[J/kg*K]
Adiabatic Exponent	κ	1,4	[-]

Sensitivity of Pressure Measurements

The sensitivity of polytropic head with varying *inlet* and *outlet* pressure is shown in respectively Figure 6.1 and Figure 6.2. The polytropic head is equally influenced, in order of relative deviation magnitude, by inlet and outlet pressure measurements.
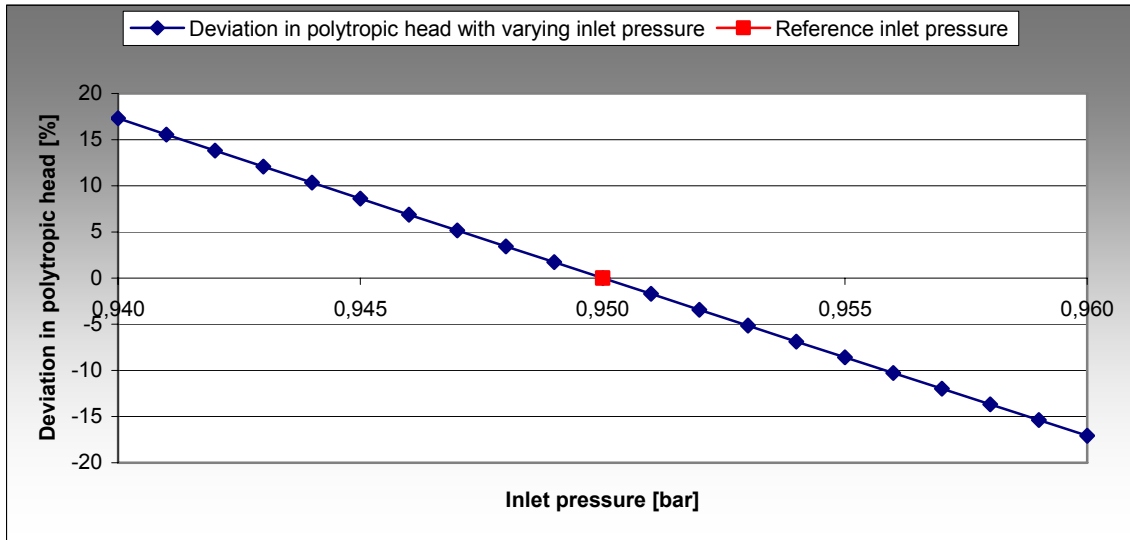
Figure 6.1: Deviation in polytropic head with variation in inlet pressure
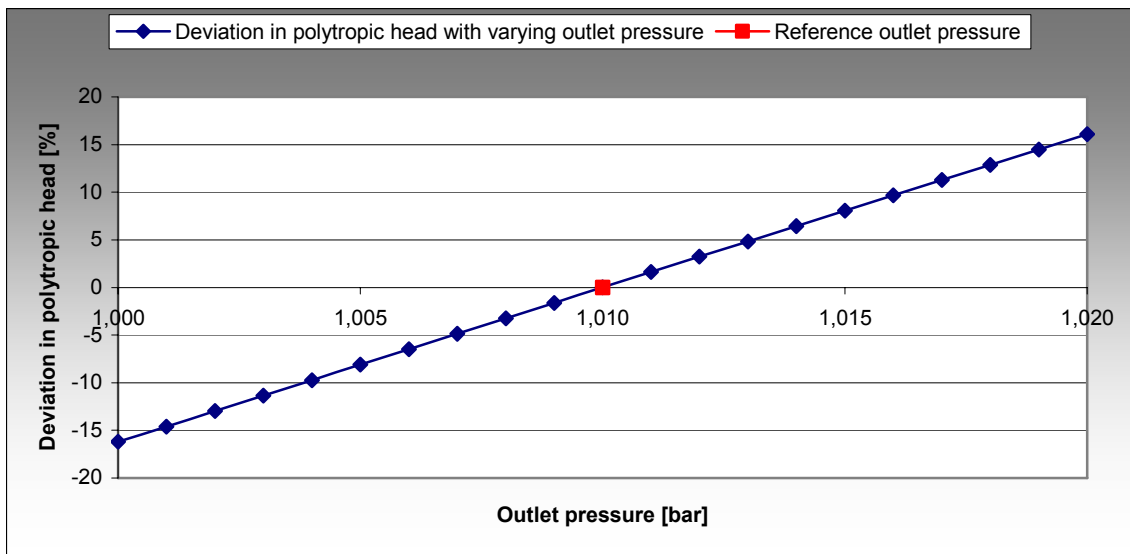
Figure 6.2: Deviation in polytropic head with variation in outlet pressure

A measurement uncertainty of 0.001 bar in inlet pressure gives a relative deviation of 1.7% for the calculated head. An equal uncertainty in outlet pressure results in a relative deviation of 1.6%, as shown in Appendix G.1.

The sensitivity analysis shows that the performance calculations for the actual compressor test and operating range are highly influenced by inaccurate measurement of inlet and outlet pressure.

A summary of the sensitivity analysis for polytropic head with variation in pressure for case 1 is shown in Table 6.3. The polytropic head deviates 1% when the inlet or outlet pressure deviate 0.061%, which corresponds to a discrepancy of 0.0006 bar. To achieve a 96% precision, the inlet or outlet pressure can deviate up to 0.245%.

Table 6.3: Sensitivity of polytropic head with varying pressure – Case 1

Hp [%]	Relative deviation			
	p_1 [%]	p_1 [bar]	p_2 [%]	p_2 [bar]
0,1	0,006	0,0001	0,006	0,0001
0,5	0,031	0,0003	0,031	0,0003
1	0,061	0,0006	0,061	0,0006
2	0,123	0,0012	0,123	0,0012
4	0,245	0,0023	0,245	0,0025

The deviation curves for polytropic efficiency are equal to the curves for polytropic head, as shown in Table G.1 and Table G.2 in Appendix G.1.

Sensitivity of Temperature Measurements

Figure 6.3 and Figure 6.4 shows the sensitivity of polytropic head with varying *inlet* and *outlet* temperature.

An uncertainty of 1.0 K in inlet or outlet temperature results in a deviation of 0.17% for the calculated polytropic head, as given in Table G.3 and Table G.4 in Appendix G.1. The sensitivity analysis shows that the polytropic head is only slightly influenced by relative deviations of inlet and outlet temperature for case 1.

The polytropic efficiency is, in contrast, highly sensitive to uncertainties in temperature measurements. Table G.3 and Table G.4, in Appendix G.1, show that a strong influence on the calculated efficiency when varying inlet and outlet temperature. A 1.18% increase in inlet temperature results in a 100% increase in polytropic efficiency.
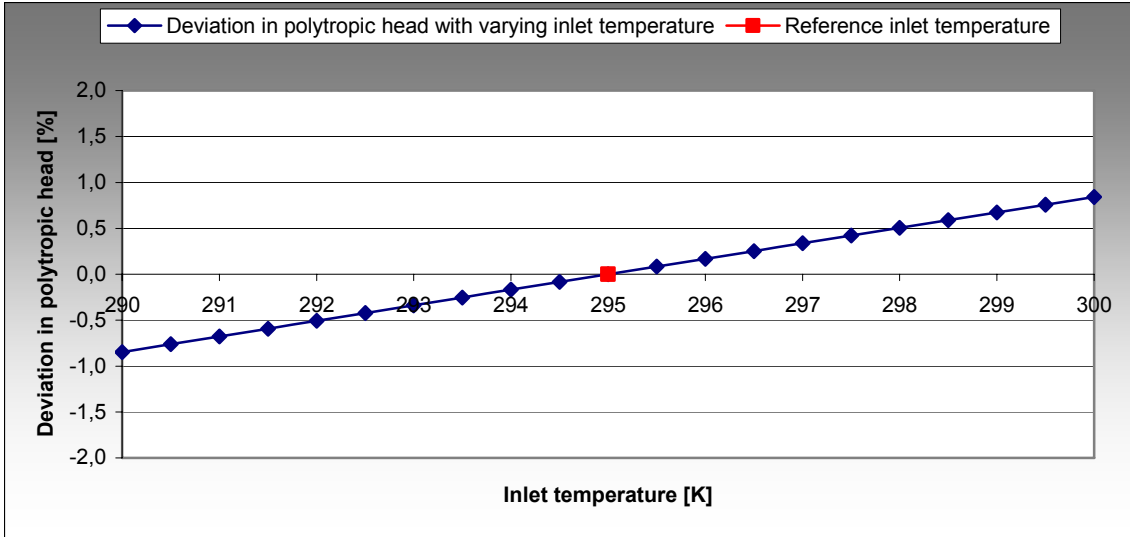
Figure 6.3: Deviation in polytropic head with variation in inlet temperature
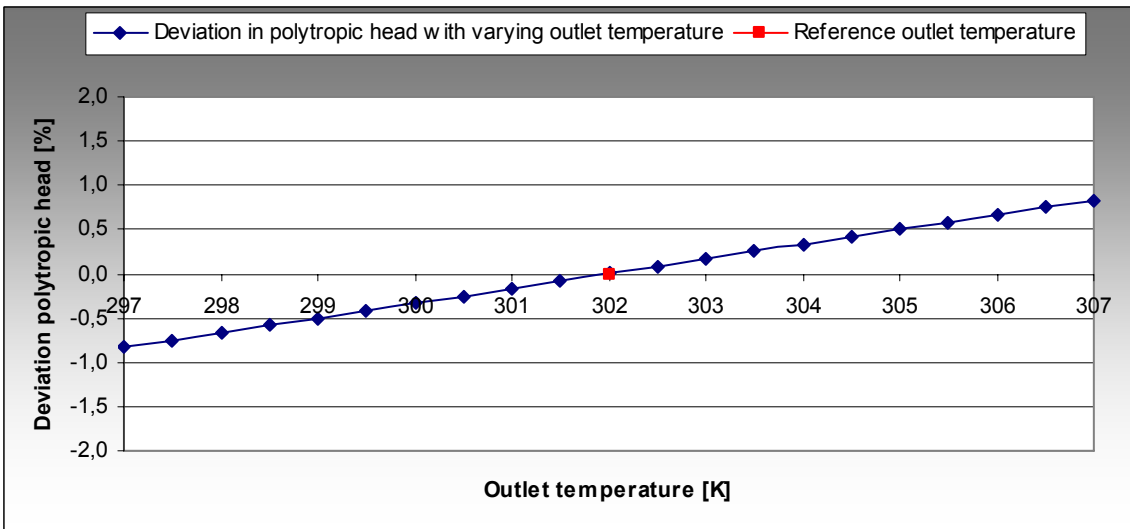
Figure 6.4: Deviation in polytropic head with variation in outlet temperature

A summary of the sensitivity analysis for polytropic head with variation in temperature for case 1 is shown in Table 6.4. The polytropic head deviates 1% when the inlet temperature deviate 2.015%, which corresponds to a discrepancy of 5.94 K. The outlet temperature can deviate up to 1.999%, 6.04 K, to achieve the same accuracy for the polytropic head. To achieve a 96% precision, the inlet temperature can deviate up to 8.138%, while the outlet temperature can deviate up to 8.073%.

Table 6.4: Sensitivity of polytropic head with varying temperature – Case 1

Hp [%]	Deviation			
	T_1 [%]	T_1 [K]	T_2 [%]	T_2 [K]
0,1	0,201	0,59	0,199	0,59
0,5	1,006	2,97	0,998	3,01
1	2,015	5,94	1,999	6,04
2	4,043	11,93	4,011	12,11
4	8,138	24,01	8,073	24,38

6.2 Case 2

Sensitivity at Higher Pressure Ratio

The test parameters used in the sensitivity analysis for case 2 are listed in Table 6.5. The constant input values are the same as for case 1. The calculated values resulting from the sensitivity analysis are shown in Appendix G.2.

Table 6.5: Reference test parameters – Case 2

Test Parameters	Symbol	Reference Test Point	Units
Inlet Pressure	p_1	0,95	[bar]
Outlet Pressure	p_2	2,00	[bar]
Inlet Temperature	T_1	295	[K]
Outlet Temperature	T_2	387	[K]

A summary of the sensitivity analysis for polytropic head with variation in pressure for case 2 is shown in Table 6.6. The polytropic head deviates 1% when the inlet or outlet pressure deviate 0.747%, which corresponds to a discrepancy of 0.0071 bar for the inlet pressure and 0.0149 bar for the outlet pressure. To achieve a 96% precision, the inlet or outlet pressure can deviate up to 3.023%.

Table 6.6: Sensitivity of polytropic head with varying pressure – Case 2

Hp [%]	Relative deviation			
	p_1 [%]	p_1 [bar]	p_2 [%]	p_2 [bar]
0,1	0,074	0,0007	0,075	0,0015
0,5	0,373	0,0035	0,373	0,0075
1	0,747	0,0071	0,747	0,0149
2	1,500	0,0143	1,500	0,0300
4	3,023	0,0287	3,023	0,0605

A summary of the sensitivity analysis for polytropic head with variation in temperature for case 2 is shown in Table 6.7. The polytropic head deviates 1% when the inlet temperature deviate 2.102%, which corresponds to a discrepancy of 6.20 K. The outlet temperature can deviate up to 1.919%, 7.43 K, to achieve the same accuracy for the polytropic head. To achieve a 96% precision, the inlet temperature can deviate up to 8.499%, while the outlet temperature can deviate up to 7.746%.

Table 6.7: Sensitivity of polytropic head with varying temperature – Case 2

	Relative deviation			
Hp [%]	T_1 [%]	T_1 [K]	T_2 [%]	T_2 [K]
0,1	0,209	0,62	0,191	0,74
0,5	1,049	3,10	0,958	3,71
1	2,102	6,20	1,919	7,43
2	4,220	12,45	3,850	14,90
4	8,499	25,07	7,746	29,98

The deviations for polytropic efficiency are highly different from case 1, as shown by the tables in Appendix G.2. For case 1 a 1.18% increase in inlet temperature results in a 100% increase in polytropic efficiency. For case 2 the same increase in inlet temperature only gives an 11.5% increase for the efficiency.

6.3 Wet Gas Considerations

The presence of liquid in a compression process may decrease the discharge temperature and specific gas volume, as described in chapter 5.7. Accurate pressure and temperature measurements are thus essential for wet gas compression analysis. The inlet fluid condition will determine the degree of evaporate cooling or condensation through the compression process. [7]

6.4 Conclusion Chapter 6

Due to the low pressures involved for the actual compressor test, the polytropic head and efficiency are highly sensitive to uncertainties in pressure measurements. The polytropic head deviates 1% when the inlet or outlet pressure deviate 0.061%. The sensitivity for polytropic efficiency is identical to the sensitivity of polytropic head for pressure measurement uncertainties.

Uncertainties in temperature measurements will only slightly influence the polytropic head for the actual test. The polytropic head deviates 1% when the inlet temperature deviates 2.015%. The outlet temperature can deviate up to 1.999% for the same deviation in head. The polytropic efficiency for case 1 is highly sensitive to uncertainties in temperature measurements. A 1.18% increase in inlet temperature results in a 100% increase in polytropic efficiency.

For a compression process with higher outlet pressure and temperature, the polytropic procedures are less sensitive. The sensitivity is particularly reduced for the polytropic efficiency. A 1.18% increase in inlet temperature results in an 11.5% increase in polytropic efficiency.

The polytropic efficiency calculated for the compressor test turned out to be extremely high, indicating that one or more parameters were measured inaccurately. The sensitivity analysis presented shows that inaccurate temperature measurements, especially at the compressor inlet, will highly influence the efficiency calculation for compressors at low pressure and temperature operating condition.

Chapter 7

7. Aerodynamic Instability

7.1 Performance Characteristics

The slope of the compressor characteristic curve is strongly influenced by the gas velocity relative to the impeller blades. For a typical backswept impeller the head increases with decreasing flow due to a reduction in relative velocity. The head increase, with decreasing flow, is what causes the basic slope to the centrifugal compressor performance curve as shown in Figure 7.1.
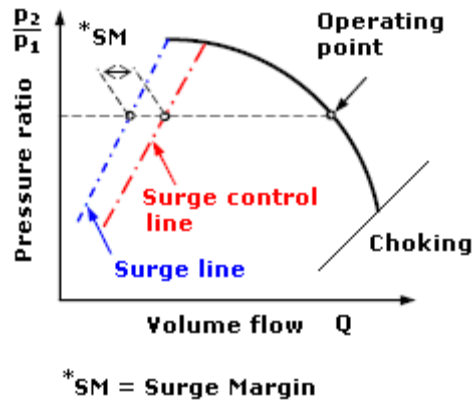
Figure 7.1: Typical centrifugal compressor characteristic

Most compressors reveal specific changes in behavior and flow pattern when operated at flow rates sufficiently below the design value. Generally a point is reached at which the pressure rise is at a maximum and further reduction in mass flow leads to a sudden change in the compressor flow pattern. The head curve will then be positively sloped and have a theoretically unstable characteristic. [16]

The centrifugal compressor characteristics are determined by the geometry of the compressor components and the compressor operating condition. Each of the compressor components will have an optimum operating condition where its losses are at a minimum. These losses will increase as the compressor operates further from the optimum operation point and hence impose definite limits on the operating range of the compressor.

The common terminology for the onset of instability is the *surge point*, regardless of the type of instability occurring in the compressor. A line showing the instability location for different rotational speeds is known as the *surge line*. The *surge line* is referred to as the compressor stability limit as shown in Figure 7.1.

A safety margin is set between the surge line and the closest allowable operating point to avoid the compressor from being directed into the surge region. The surge margin, denoted *SM* in Figure 7.1, is usually set to 10% from the surge line. [17] The surge margin ensures stable operation of the compressor but may prohibit operation in regions of highest efficiency or pressure rise.

7.2 Instability Mechanisms

The efficiency and performance of a compressor are constrained by aerodynamic instabilities. Flow instabilities limit the stable operating range and may prohibit operation in regions with highest efficiency. In addition to the adverse performance effects, flow instabilities may cause unacceptable levels of subsynchronous rotor vibration. [18]

Flow instabilities are perturbations of the steady, axis-symmetric flow during normal operating conditions. The instability mechanisms are commonly divided into three categories; *stall, rotating stall* and *surge*. Stall and rotating stall are unsteady propagation of flow fluctuations limited to one or few components of a compressor, while surge accompanies the propagation and resonance of fluctuations throughout a compressor system.

Surge

Surge is a system phenomenon that may occur in compressors due to changes in operating conditions. Surging is associated with full flow reversal and fluctuations in inlet and discharge pressure and temperature. This essentially one-dimensional instability can results in a limit cycle oscillation in the compressor characteristic depending on the amplitude of flow and pressure fluctuations as shown in Figure 7.2.

Surge may be classified according to the amplitude of the flow fluctuation. "*Deep surge*" usually refers to the condition when full flow reversal occurs. The aerodynamic pulsation caused by surging is transmitted throughout the compression system.

Operation during surge may result in extensive loss of performance and efficiency. Flow reversal may in addition result in reverse bending on compressor components and high radial and axial vibrations.
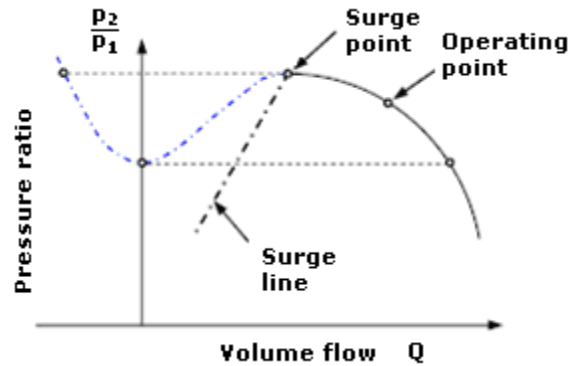
Figure 7.2: Compressor characteristic with surge cycle

Stall

Stall is a local instability phenomenon in which a region of stagnant flow occurs within one or few components of the compressor. Stationary stall cells form in vaned diffusers, return channels, guide vanes etc. The phenomenon may occur at any point on the compressor characteristic curve but is more common at very high or very low flow rates. [19]

Rotating Stall

Rotating stall refers to the class of stall cells in which one or more regions of stagnant flow rotate around the circumference of the compressor. The most common forms of rotating stall occur in impellers or diffusers at very low flow rates. [19]

Both impeller and diffuser rotating stall can have significant effects on mechanical and aerodynamic performance. The flow separation and the high losses associated with stall cells may result in degraded performance. [20] Rotating stall cells may in addition subject the rotor to unbalanced pressure forces and hence cause unacceptable levels of subsynchronous vibration of the rotor. [18]

Impeller Rotating Stall

There exist numerous theories in the literature to the nature and origin of impeller rotating stall. Probable causes of the phenomenon are flow separation near the impeller exit, high incidence angles at the impeller leading edge or pressure disturbances caused by the impeller blade geometry.

Off-design operation changes the incident angle to the impeller blades and flow separation may occur. Breakdown of the flow in one impeller channel will cause a deflection to the incoming flow. The deflection will cause the incidence to increase to one side and reduce it on the other. The blade with increased incidence will tend to stall

at the suction side of the blade leading edge. [20] The flow separation will continuously shift around the impeller blades in the direction in which incidence are increased as shown in Figure 7.3.
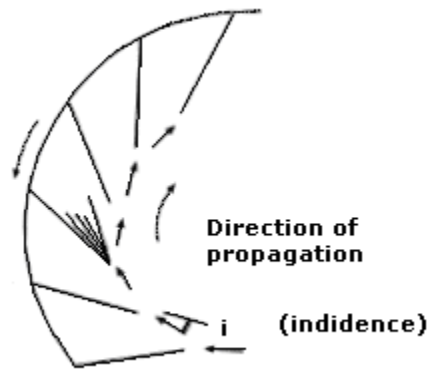
Figure 7.3: Rotating stall in a centrifugal impeller [17]

Diffuser Rotating Stall

Compressor performance during rotating stall is often dominated by the flow field in the diffuser, which may be highly non-uniform [21] There is always a tendency for the flow to break away from the boundary in a diffusing process and hence the radial diffuser has an important role in establishing the overall efficiency and pressure-rise of a centrifugal compressor. The diffuser may be the component limiting the operating range, depending on the diffuser design and it's matching to the impeller. A distorted flow field from the impeller will affect the diffuser inlet condition and hence have a strong effect on compressor performance in the unstable operating region. [21]

The pressure field in the diffuser inlet is highly sensitive to changes in flow rate. [16] The onset of diffuser rotating stall is strongly influenced by the diffuser flow angle, which is a function of the diffuser geometry, gas Reynolds Number and compressor operating conditions. [21] The diffuser flow path is shown in Figure 7.4.
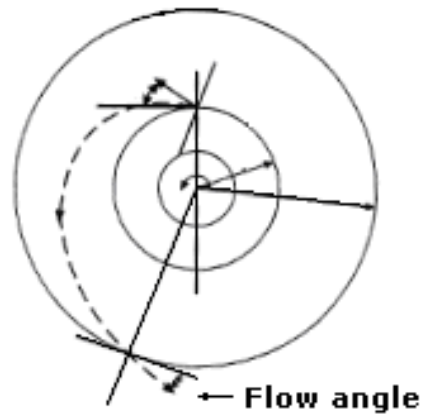
Figure 7.4: Flow through a vaneless diffuser [17]

When the flow angle exceeds some critical angle, the diffuser walls will dissipate the flow momentum of the gas by friction to the point where frictional forces are increasing faster than the compressor head. The growth in boundary layer thickness results in increased blockage in the diffuser channels. The diffuser pressure recovery and stability decreases as inlet blockage increases. [22] Off-design operation continuously changes the diffuser flow angle and results in periodic flow unsteadiness in the diffuser inlet.

Matching between Components

Instability phenomena are often more complicated in radial compressors due to matching between compressor elements. The more disturbed the impeller exit flow profile, the greater the likelihood that the downstream diffuser will stall. Stall cells formed in the diffuser may excite the formation of rotating stall in the impeller. [21]

Rotating stall usually occurs prior to surge, but may also exist in the nominally stable operating range. [18] Surge is usually the flow instability that is of most concern in centrifugal compressors since the centrifugal compressor may operate fairly satisfactory with rotating stall present. Analyzing the instability effect of each compressor component is important to determine the total system instability.

7.3 Wet Gas Impact on Compressor Stability

The presence of liquid will alter the flow regime within the compressor. Multiphase flow within wet gas compressors is expected to be annular due to the high gas volume fraction and the high flow velocity involved. [23] The annular flow pattern will consists of a thin liquid film and dispersed droplets in the core gas flow.

Identification of the liquid distribution is highly important in understanding the different mechanisms leading to compressor instability. Multiphase flows in compressors have complicated characteristics including interfacial interactions and relative movement between phases. [23]

Several parameters are considered to influence the onset and severity of compressor instability when exposed to wet gas. A reduced stall margin is expected in wet gas compression due to premature boundary layer separation. The interface between the gas and liquid film is characterised by a pattern of waves introducing an additional roughness to the flow. [23] Increased blockage induced by the roughness result in a reduced flow area and premature boundary layer separation. [23] Premature separation will impose considerable limitation on the stability margin and hence on the operational characteristic of the compressor. Recovery of potential energy in the diffuser will in addition be highly disturbed by the liquid particles and premature boundary layer separation. [23]

Changes in compressor velocity distribution and flow angles contribute to reducing the stability margin by inducing high Mach numbers. High Mach numbers are associated with the possibility of aerodynamic shock waves followed by increased boundary layer separation.

7.4 Test Procedure

Pressure fluctuations caused by instabilities and the resulting vibration of the rotor should be measured with variation of flow rate and impeller rotating speed to document the different instability phenomena.

The surge line should be approached slowly, by throttling suction or discharge flow while maintaining compressor speed. The compressor flow rate should be varied from near surge to choke conditions to evaluate the entire operating range of the compressor.

Determination of head, flow and efficiency close to the surge line may be highly inaccurate due to fluctuating measurement readings.

7.5 Instrumentation

Dynamic Pressure Measurements

Dynamic pressure transducers should be installed in the inlet and outlet piping for detection of pressure pulsations throughout the compressor system.

In order to investigate the unstable characteristics within different compressor components, internal instrumentation should be implemented. Circumferentially distributed pressure transducers at the locations shown in Figure 7.5 are recommended.
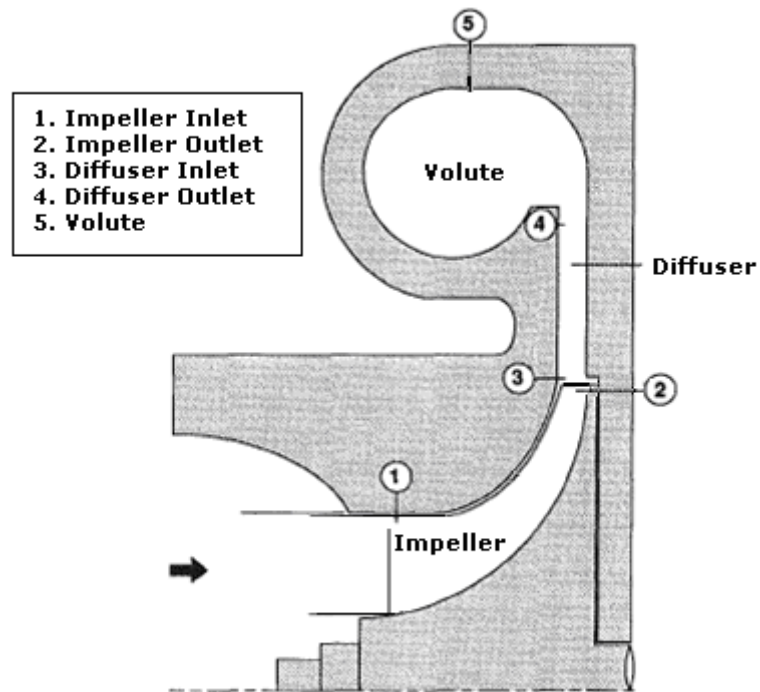
Figure 7.5: Measurement locations for internal instrumentation [24]

The recommended positions for the pressure transducers at the entrance to the vaneless diffuser, position 3, are shown in Figure 7.6. [24] Due to narrow flow channels in the compressor the sensors must have as small dimensions as possible and be flush mounted in the shroud wall to minimize disturbances accumulated from the installed sensors.
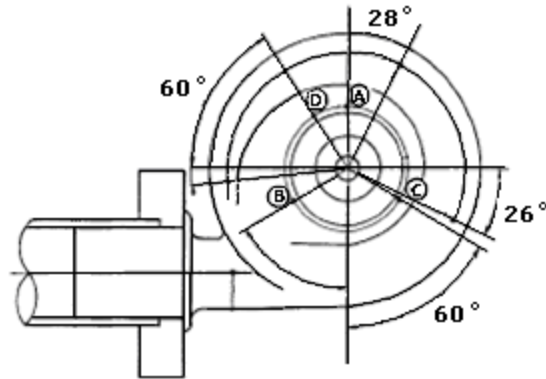
Figure 7.6: Circumferential measuring positions in the diffuser [24]

Measurement of Radial Vibration

Vibration probes installed at each end of the rotor are recommended to obtain measurements of the rotor vibration. The Kitsler sensors are suitable for such measurements.

7.6 Pressure Characteristic Analysis

The pressure characteristics can be utilized to document the compressor behavior and to indicate whether surge or rotating stall occur. Compressor surge appear as large high to low pressure fluctuations in the pressure characteristic at compressor inlet/discharge, whereas rotating stall displays fluctuations more frequently, as shown in Figure 7.7.
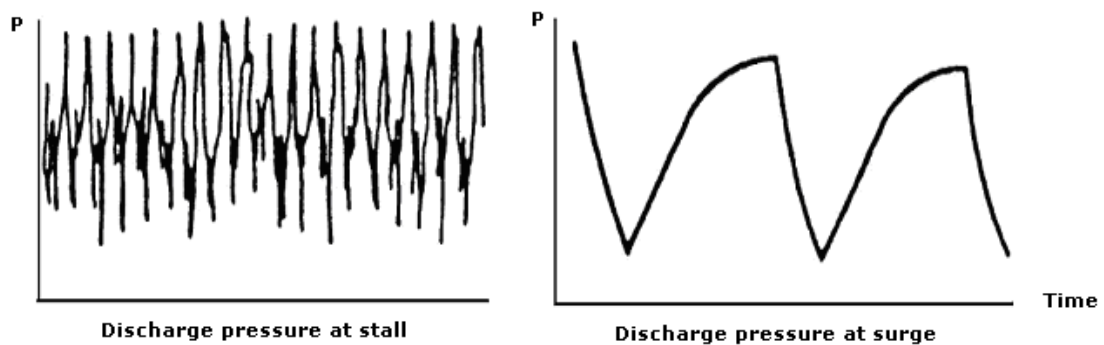
Figure 7.7: Stall and surge pressure characteristics at compressor inlet/discharge

Figure 7.8 shows a typical pressure characteristic. An indication of rotating stall is seen as steadily increasing pressure amplitude just prior to the first surge cycle.
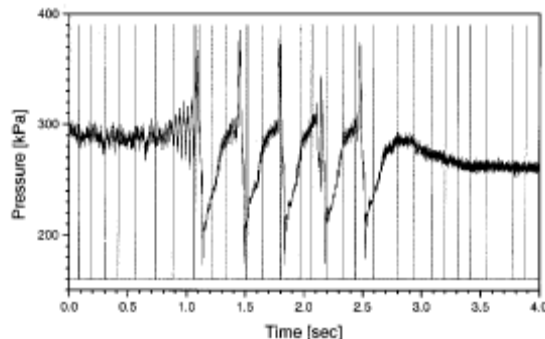
Figure 7.8: Pressure fluctuations with time [25]

Since rotating stall is a local pressure disturbance, in contrast to surge which cause fluctuations throughout the compressor system, pressure characteristic deduced from internal measurements within a diffuser can determine the type of instability that occur. Surge differs from rotating stall by simultaneous occurrence of high to low pressure fluctuations on all the pressure transducers located circumferentially in the diffuser.

7.7 Frequency Spectrum Analysis

Pressure Fluctuation Frequency

The frequency content of a pressure reading can be analyzed by utilizing a fast Fourier transformation (FFT). The relative magnitude of the dominant instability frequency is compared to the magnitude related to the blade passing frequency to determine type of instability that is present. [26] Rotating stall appears as a broad and varied peak at more than one frequency in the FFT spectrum, whereas surge is seen as a distinct frequency. [26]

Radial Vibration Frequency

M. Kita et al. [18] found a correlation between the pressure fluctuation and the rotor vibration during rotating stall. The rotor vibration amplitude is proportional to the pressure fluctuation amplitude and may therefore be an indication of compressor instability. The increased vibration is in most cases due to the onset of rotating stall rather than full surge.

Impeller and diffuser rotating stall generally manifest themselves in different frequency ranges. By analyzing the frequency spectrum of the radial vibrations one may identify the

type of rotating stall that occurs. The subsynchronous radial vibration frequency for impeller rotating stall lies in the range of 50-80% of the compressor running speed, while the range for diffuser rotating stall is 6-33%. [19]

A determination of whether the radial vibration is flow sensitive can be an indicator when identifying the flow instabilities. There will be a distinct flow rate at which the impeller rotating stall will come and go. Unlike when impeller stall is present, diffuser rotating stall will appear at some distinct flow rate but will not disappear by some reduction in flow rate. A significant increase in flow rate is necessary to get rid of the stall cells.

Since various rotordynamic elements may yield vibration signals that approximate stall characteristics, it is important to rule out such rotor effects before attributing subsynchronous rotor vibration to rotating stall. [19] Vibration due to rotordynamic elements can be observed with relatively constant response frequency despite changes in discharge pressure, in contrast to instability caused vibration.

7.8 Conclusion Chapter 7

The efficiency and performance of a compressor are constrained by aerodynamic instabilities. In addition to the adverse performance effects, instabilities may cause unacceptable levels of subsynchronous rotor vibration. A reduced stall margin is expected in wet gas compression due to premature boundary layer separation.

Pressure fluctuations caused by instabilities and the resulting vibration of the rotor should be measured with variation of flow rate and impeller rotating speed to document the different instability phenomena over the entire compressor operating range.

Dynamic pressure transducers in the inlet and discharge piping are recommended for detection of pressure pulsation throughout the compressor system. Circumferentially distributed pressure transducers at different locations within the compressor components are recommended to document the internal flow behavior. Vibration probes installed at each end of the rotor are recommended to obtain vibration measurements.

By analyzing the frequency spectrum for the pressure fluctuations and radial vibrations one can identify the cause and type of instability phenomenon that occurs. The frequency content can be analyzed by utilizing a fast Fourier transformation (FFT). Rotating stall appears as a broad and varied peak at more than one frequency in the FFT spectrum, whereas surge is seen as a distinct frequency. [26] The subsynchronous radial vibration frequency for impeller rotating stall lies in the range of 50-80% of the compressor running speed, while the range for diffuser rotating stall is 6-33%. [19]

Chapter 8

8. Multiphase Flow Measurements and Visualization Techniques

Complex flow structure with local randomness is characteristic in multiphase flow systems. The understanding of such complex flow patterns requires reliable data over the entire flow field, which in turn depends on the implementation of proper measuring and visualization techniques.

Visualization techniques with careful control of the flow distribution are desired in wet gas compression to document aerodynamic instability under various compressor operating conditions and to identify the dynamic changes occurring in the flow field prior to rotating stall and surge.

Techniques commonly used for visualization of single-phase flows may be difficult to implement in multiphase compressors due to the inherent non-homogeneity of the multiphase flow field. A thorough evaluation of the visualization techniques is essential to outline their range of applicability, along with advantages and limitations inherent to each technique.

8.1 Direct Visualization

Direct visualization of the flow field may provide useful information about the flow behavior within the compressor components. Identification of the mechanism leading to degraded performance and operational limitations may be obtained by rendering certain flow characteristics directly accessible to visual perception. The prevalent flow regime, the liquid distribution, and the interaction between the phases can then be documented and further analyzed.

The compressor flow field can be visualized directly by replacing sections of the compressor casing with transparent material, Plexiglas, as shown in Figure 8.1.
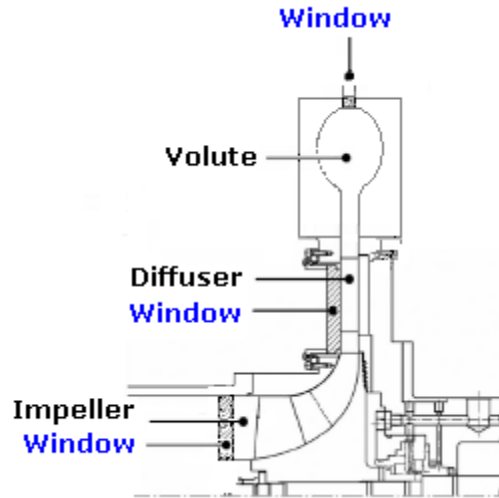
Figure 8.1: Locations for transparent windows

Since the compression fluid is transparent and its flow pattern may not be seen directly, an injection of particles or dye which scatters light should be inserted to better visualize the fluid motion.

A high-speed camera that captures the scattered light from the particles can be used to reconstruct a stereoscopic view of the flow. Quantitative data from the flow field can be derived by analyzing the obtained picture. Computers that allow calculation in reasonable time, and with the high number of operations required by image processing, must be utilized.

High seed particle concentration is recommended for compressor flow field studies since high spatial resolution measurements are required. [25] Determination of optimal particle size and density is a major challenge when utilizing tracer particles for flow visualization in compressors. The particle size should be small enough to accurately follow the flow through the compressor channels. The difference between the fluid and the particle motion can be minimized by giving the particles a density almost coinciding to that of the fluid. The method gives accurate results in stationary flow, but may fail in unsteady and transient flows due to the finite size of the particles.

A disadvantage with particle tracer methods is that the injection process and the injected material may influence the flow field. Flush-mounted injection probe in a close distance to the measuring point will minimize the probe disturbances. Window deposition of particles is an obstacle to tracer-based measurement techniques since the seeding particles have a tendency to adhere to the transparent windows.

Multiphase Application

The observer may not be able to fully visualize the different wet gas flow phenomena due to liquid film formation on the Plexiglas windows. The liquid deposition on the transparent windows depends on the GVF and the relative concentration of dispersed droplets in the gas core flow.

Particle tracer methods in wet gas compression have a challenge owing to the varying density of the phases involved and to the turbulent and unsteady state of the fluids. This difficulty is further discussed in chapter 8.2 when laser measurement techniques are addressed for multiphase applications. An idea of the origin and development of the flow regime and phase distribution can nevertheless be obtained.

8.2 Laser Measurement Techniques

Laser measurement techniques are suitable for flow investigation in the narrow flow channels of a centrifugal compressor. [27] Velocimetric measurements within a centrifugal impeller, diffuser and volute can provide information of the main features of the fluid flow. The volume in which the measurements are made is only limited by optical means so that measurements can be made even in boundary layers and at places that cannot be reached by probes.

Laser measurement techniques are limited to transparent measurement locations. Optical access to the internal flow of a centrifugal compressor can be provided as described for direct visualization. Figure 8.2 shows an optical window utilized for PIV measurements in a vaned diffuser. The technical limitations caused by the surrounding of the compressor may be an obstacle when implementing the optical apparatus.
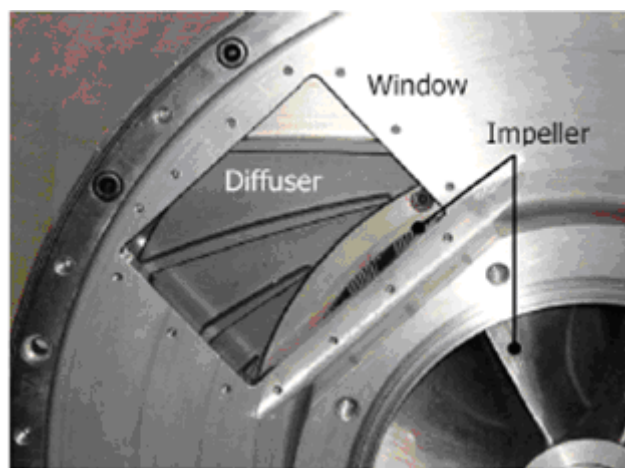
Figure 8.2: Test section of a diffuser with an optical window [28]

Laser velocimeters enable non-intrusive measurements of the flow field. Unlike the probe measurement methods, the laser velocimetric measurements are independent of the properties of the fluid and environmental conditions such as temperature, pressure and density.

Laser Doppler and Laser two-focus Velocimetry

Laser Doppler Velocimetry (LDV) and Laser two-focus velocimetry (L2F) have been widely used for flow measurements in compressors. LDV is a technique for measuring the direction and speed of fluids. By analyzing the Doppler-equivalent frequency of the laser light scattered by the seeded particles within the flow, the velocity field of the fluid can be determined.

Laser-two-focus measurements (L2F) collects light scattered from particles convected by the flow. The time-of-flight of the particles between two focused laser spots is measured. In contrast to the LDV, the L2F velocimetry is a statistical based measurement system; hence the temporal fluctuations of the flow cannot be measured.

Particle Image Velocimetry

Particle Image Velocimetry, PIV technique, has major features of other velocimetric methods. The technique can present extensive velocity fields in a very short time and can provide simultaneous and multipoint measurements. Hayami et al. [27] performed detailed flow measurements within a centrifugal impeller using PIV. Ibaraki et al. [28] applied PIV for vaned diffuser measurements.

PIV is an imaging technique used to measure instantaneous velocities and related properties in fluid flows. The PIV method measures the velocity components across a planar 2D matrix of points within a flow field in order to produce a 2D velocity vector field.

The fluid must be seeded with tracer particles assumed to accurately follow the flow. By illuminating the particles with a laser light sheet, an instantaneous image is produced. The positions of the moving particles are recorded with a CCD camera.

To obtain velocity information the laser must be pulsed at least two times at a known time separation, creating an image of the laser light sheet in which the particles appear as multiples spots. The separation of the recorded spots is a measure of the distance traveled by the particles between the laser light pulses.

Typical PIV apparatus consists of a digital camera, a high power laser, for example a double-pulsed Nd:YAG laser and an optical arrangement to convert the laser output light to a light sheet. A PIV measurement system located at the compressor inlet in shown in Figure 8.3.
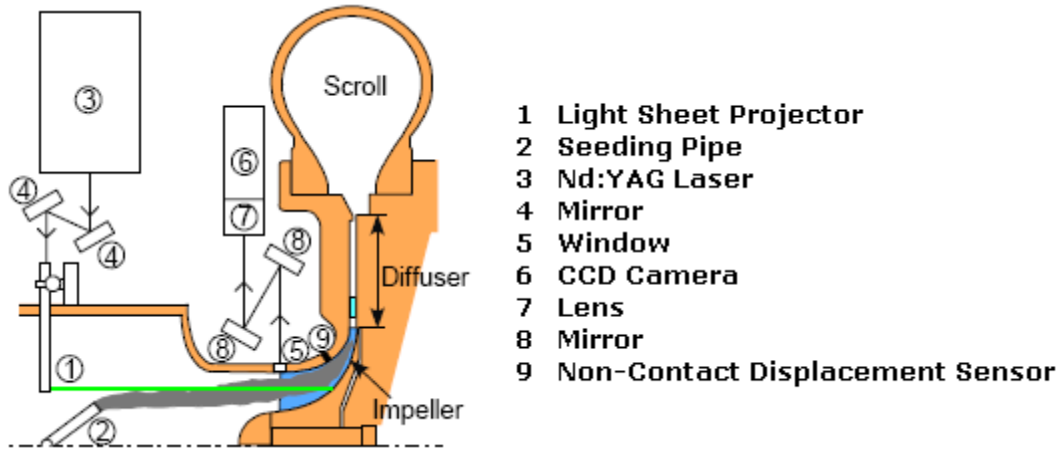
Figure 8.3: PIV measurement system [29]

Multiphase Application

Laser measurements within wet gas compressors are more challenging than for single-phase compressors. Liquid film formation and possible window deposition of particles during the compressor testing can prevent a clear optical path to the measurement zone.

No particle seeding is required if the dispersed phase itself is the object of interest. [30] Optical properties such as light refraction changes in sections within the flow where there are big local differences in flow density. Fluid density is a function of the refractive index of the flowing medium, which is a measure of how much the speed of light is reduced inside the medium.

If the phase velocities are to be independently measured, to determine local slip velocities and superficial velocities, the gas flow must be seeded and some discrimination between the seed particles and the dispersed phase is necessary. [30]

A velocity map of the flow field can be obtained from PIV measurements, but it may be difficult to identify which velocity vectors correspond to which phase of the flow. Towers et al. [31] examined the use of fluorescent particles for two-phase flow measurements. The technique operates by identifying fluorescent tracer particles inserted in one phase of the flow in order to separate the particle images obtained from both phases. Fluorescent tracer particles are appropriate for high speed unsteady gas flows and hence appropriate for studying non-stationary flow field during compressor surge. [30]

PIV measurements at the compressor inlet can give an indication of the phase behavior, liquid distribution and possible development of the flow field. PIV apparatus are more easily implemented at the compressor inlet, in contrast to compressor components downstream, due to insufficiently supply of seeding particles downstream. The measurements may in addition be more accurate at the inlet due to the highly disturbed and transient flow field in the downstream components.

69

8.3 Pressure Sensitive Paint Measurement Technique

Pressure Sensitive Paint (PSP) techniques can be adopted for detailed measurements in the compressor components where optical access is limited. Visualization of the unsteady pressure field in the diffuser at stall and surge conditions will provide useful information when documenting compressor aerodynamic instabilities. Figure 8.4 shows a typical PSP measurement system.

1	UV Lamp
2	Optical Fiber
3	Dichroic Mirror
4	Mirror
5	Window
6	High-Pass Filter
7	Lens
8	CCD Camera
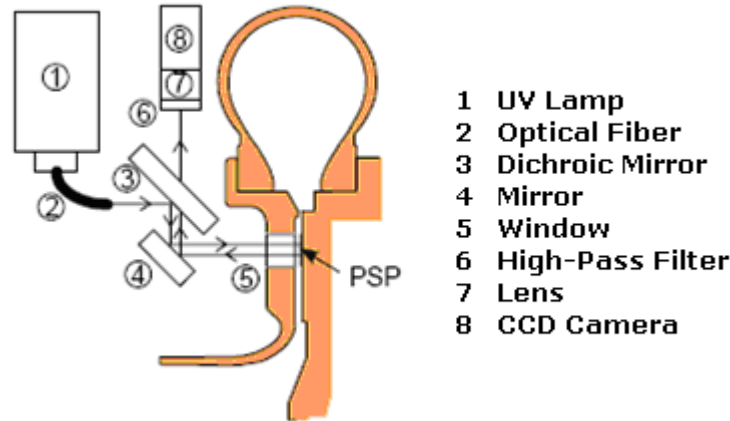
Figure 8.4: PSP measurement system [29]

PSP consists of luminescent molecules dispersed in an oxygen permeable binder. The mixture is applied to the compressor surface under investigation. Ultraviolet light is beamed onto the surface, raising the molecules to a higher energy level. The binder emits light at a visible and longer wavelength to return to the original energy state. A CCD camera, capturing the intensity of emission from the luminescent molecules, as shown in Figure 8.5, obtains images of the surface pressure distribution. The small size of the PSP molecules allows for detailed pressure data to be obtained inside the diffuser.

PSP measurements exploit the oxygen sensitivity of the luminescent molecules dispersed within the binder. [32] The excited molecules are deactivated with oxygen, making the emission intensity proportional to the amount of oxygen in the nearby environment. Higher pressures fields mean that more oxygen molecules are being squeezed into the flow which means lower intensity of light being emitted.

The Stern-Volmer equation, given in equation (8.1), can be used for intensity-based measurements. The calibration coefficient A and B are temperature-dependent and can be obtained experimentally for a given PSP formulation. [32]

$$I_{ref} = A(T) + B(T)\frac{p}{p_{ref}}$$ (8.1)
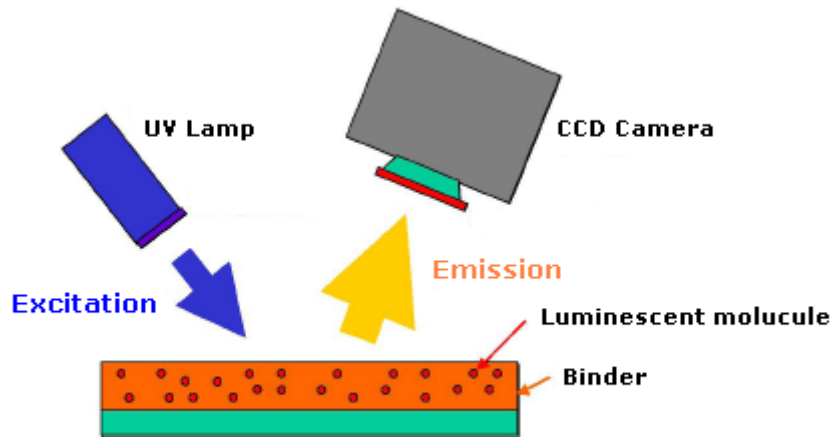
Figure 8.5: The schematic PSP measurement

Multiphase Application

There are some probable difficulties when utilizing the PSP technique for visualization in a wet gas compressor. Liquid film formation on the optical window and on diffuser surface will influence the intensity-based measurements. Dispersed droplets in the gaseous phase are likely to disturb the excitation and emission of light and adversely affect the achievable measurement accuracy.

An incompressible liquid film on the binder surface can hinder the oxygen sensitive molecules to react to different pressure levels. The intensity of the emitted luminescence captured by the CCD camera will then be inaccurate due to the reduced amount of oxygen available to deactivate the exited molecules.

8.4 CFD

Computational fluid dynamics (CFD) uses numerical methods and algorithms to simulate and analyze behavior of fluids under a wide range of conditions. The objective is to analyze the simulated vector field to identify features such as turbulence, vortices, and other forms of structure in the compressor flow field. Computers are utilized to perform the calculations required to simulate the interaction of fluids and gases in a complex flow field.

Although computational fluid dynamics can obtain predictive solutions for the complex flow pattern in compressors, experimental measurement should always be performed to validate the computed values.

8.5 Conclusion Chapter 8

Visualization of the flow field can provide useful information about the flow behavior within the compressor components. Pressure and velocity fluctuations caused by aerodynamic instabilities can be measured and visualized to document instability phenomena.

The visualization methods presented require optical access to the internal flow. This can be accomplished by replacing sections of the compressor casing with Plexiglas. Liquid film formation on the Plexiglas windows may prevent this optical access and cause inaccurate measurements when utilizing the techniques in wet gas compressors.

Laser measurement techniques are recommended for flow investigation in centrifugal compressors. PIV techniques can present extensive velocity fields in a very short time and can provide simultaneous and multipoint measurements, which is of importance when documenting aerodynamic instabilities.

No particle seeding is required if the dispersed phase itself is the object of interest. If the phase velocities are to be independently measured, the gas flow must be seeded and some discrimination between the seed particles and the dispersed phase is necessary. Fluorescent tracer particles are recommended for investigating the non-stationary flow field during both single- and multiphase compressor instability.

PSP measurements are suitable for obtaining information of the pressure distribution during single-phase compression, but will be highly inaccurate for wet gas applications. The intensity-based measurements will be influenced by liquid film formation on the binder surface and disturbed by the dispersed droplets in the gaseous phase.

Chapter 9

9. Conclusion

The ideal polytropic performance analysis is suitable for the actual compressor test. The values estimated for the polytropic exponent and polytropic head by PRO/II agree closely with the calculated values determined from the ideal gas equations and thus verify the use of ideal polytropic calculation procedures for the compressor test.

When converting the performance results for the compressor test to real gases at high pressure and temperature conditions, the ideal assumptions will not be applicable. The sensitivity of the ideal polytropic head with deviations in polytropic exponent is notably low for the actual compressor test, but will be substantially higher for greater pressure ratios. The Schultz polytropic analysis must then be utilized to achieve accurate results.

The probability for phase changes to occur is limited for the planned wet gas compressor test due to the low compressor pressure ratio and the atmospheric inlet condition, and can thus be neglected in the performance evaluation. Performance procedures based on polytropic assumptions will then be accurate. For higher pressure ratios and with real gases the direct integration procedure must be implemented to account for any phase transitions along the compression path.

The polytropic efficiency calculated for the compressor test turned out to be extremely high, indicating that one or more parameters were measured inaccurately. The sensitivity analysis presented shows that inaccurate temperature measurements, especially at the compressor inlet, will highly influence the efficiency calculation for compressors at low pressure and temperature operating condition.

The polytropic head and efficiency are highly sensitive to uncertainties in the pressure measurements. The polytropic head deviates 1% when the inlet or outlet pressure deviate 0.061%. Uncertainties in temperature measurements will only slightly influence the polytropic head, but have great influence on the polytropic efficiency. The polytropic head deviates 1% when the inlet temperature deviate 2.015%. The outlet temperature can deviate up to 1.999% for the same deviation in head. A 1.179% increase in inlet temperature results in a 100% increase in polytropic efficiency.

For a compression process with higher outlet pressure and temperature, the polytropic procedures are less sensitive. The sensitivity is particularly reduced for the polytropic efficiency. A 1.18% increase in inlet temperature results in an 11.5% increase in polytropic efficiency.

A reduced stall margin is expected in wet gas compression due to premature boundary layer separation. In addition to the adverse performance effects, instabilities may cause unacceptable levels of subsynchronous rotor vibration.

The pressure fluctuations caused by instabilities and the resulting vibration of the rotor should be measured with variation of flow rate and impeller rotating speed to document the different instability phenomena over the entire compressor operating range. The frequency content can be analyzed by utilizing a fast Fourier transformation (FFT).

Dynamic pressure transducers in the inlet and discharge piping are recommended for detection of pressure pulsation throughout the compressor system. Circumferentially distributed pressure transducers at different locations within the compressor components are recommended to document the internal flow behavior. Vibration probes installed at each end of the rotor are recommended to obtain vibration measurements.

Pressure and velocity fluctuations caused by aerodynamic instabilities can be visualized to document instability phenomena. Laser measurement techniques are recommended for flow investigation in centrifugal compressors. PIV techniques can present extensive velocity fields in a very short time and can provide simultaneous and multipoint measurements, which is of importance when documenting aerodynamic instabilities.

Optical access can be accomplished by replacing sections of the compressor casing with Plexiglas. Fluorescent tracer particles are recommended for investigating the non-stationary flow field during both single- and multiphase compressor instability. No particle seeding is required if the dispersed phase itself is the object of interest. If the phase velocities are to be independently measured, the gas flow must be seeded and some discrimination between the seed particles and the dispersed phase is necessary.

Chapter 10

10. Recommendations for Further Work

Since only one test at part-load has been conducted, several tests at part- and full-load must be carried out to document and validate the performance procedure over the entire operating range.

The effects and causes of measurement uncertainties should be further investigated in order to increase the accuracy of the performance calculations.

At higher pressures and temperatures the ideal polytropic performance analysis is not suitable for the evaluation of the compressor. The Schultz calculation procedures should be implemented in the performance analysis to render possible a direct comparison of the compressor performance at different operating conditions.

Testing at wet gas conditions must be conducted to determine the accuracy and validity for the performance procedures and measurements techniques. In order to determine the suitability for the performance procedures, the GERG equation of state should be implemented and validated for wet gas applications.

By implementation of dynamic pressure transducers and PIV apparatus, additional insight into the origin and cause of flow instabilities can be obtained.

Bibliography

[1]   American Society of Mechanical Engineers, "*Performance Test Code on Compressors and Exhausters*", ASME PTC 10, 1997

[2]   S.C. Amundsen, "*Wet Gas Compression*", NTNU, Project Thesis, 2008

[3]   J.M. Øverli, "*Strømningsmaskiner*", Termiske maskiner, Bind 3, 1992

[4]   International Organization for Standardization, "*Turbocompressors – Performance test code*", ISO 5389:1992, 1992

[5]   J.M. Schultz, "*The Polytropic Analysis of Centrifugal Compressors*", Journal of Engineering for Power, pp. 69-82, 1962

[6]   Ø. Hundseid, L.E. Bakken, T. Helde, "*A Revised Compressor Polytropic Performance Analysis*", ASME GT2006-91033, 2006

[7]   Ø. Hundseid, L.E. Bakken, "*Wet Gas Performance Analysis*", ASME GT2006-91035, 2006

[8]   C. Twu, H. Kusch, "*Selection of Equations of State Models for Process Simulator*", Simsci Inc., 1994

[9]   R. Kurz, K. Brun, D.D Legrand, "*Field Performance Testing of Gas Turbine Driven Compressor Sets*", Proceedings 28th Texas A&M Turbomachinery Symposium, 1999

[10]   American Society of Mechanical Engineers, "*General Instructions*", ASME PTC 1, 1999

[11]   American Society of Mechanical Engineers, "*Test Uncertainty*", ASME PTC 19.1, 1998

[12]   American Society of Mechanical Engineers, "*Pressure Measurement*", ASME PTC 19.2, 1998

[13]   International Organization for Standardization, "*Measurement of Fluid Flow by Means of Pressure Differential Devices Inserted in Circular Cross-Section Conduits Running Full*", ISO 5167-1:2003, 2003

[14]   M.J. Moran, H.N. Shapiro, "*Fundamentals of Engineering Thermodynamics*", 5th Edition, 2004

[15]   L.E. Bakken, "*Status og utfordringer innen flerfase maskiner*", Norske Sivilingeniørers Forening, 1993

[16]   R. Hunziker, G. Gyarmathy, "*The Operational Stability of a Centrifugal Compressor and Its Dependence on the Characteristics of the Subcomponents*", ASME Journal of Turbomachinery, Vol. 116, 250-257, 1994

[17]   M.T. Gresh, "*Compressor Performance: Aerodynamic for the User*", Newnes, 2001

[18]   M. Kita, S. Iwamoto, D. Kiuchi, R. Kawashita, "*Prediction of Subsynchronous Rotor Vibration Amplitude Caused by Rotating Stall*", Proceedings of the Thirty-seventh Turbomachinery Symposium, 97-102, 2008

[19]   J.M. Sorokes, "*Rotating Stall – An Overview of Dresser-Rand Experience*", Dresser-Rand

[20]   H.I.H. Saravanamutto, H. Cohen, G.F.C Rogers, "*Gas Turbine Theory*", 5th edition, 2001

[21]   K.U. Ziegler, H.E. Gallus, R. Niehuis, "*A Study on Impeller-Diffuser Interaction – Part I: Influence on the Performance*", ASME Journal of Turbomachinery, Vol. 125, 173-182, 2003

[22]   V.G. Filipenco, S. Deniz, J.M. Johnston, E.M. Greitzer, N.A. Cumpsty, "*Effects of Inlet Flow Field Conditions on the Performance of Centrifugal Compressor Diffusers: Part 1 - Discrete-Passage Diffuser*", ASME Journal of Turbomachinery, Vol. 122, 1-10, 2000

[23]   T.G. Grüner, L.E. Bakken, L. Brenne, T. Bjørge, "*An Experimental Investigation of Airfoil Performance in Wet Gas Flow*", ASME GT2008-50483, 2008

[24]   S. Mizuki, Y. Oosawa, "*Unsteady Flow within Centrifugal Compressor Channels Under Rotating Stall and Surge*", ASME Journal of Turbomachinery, Vol. 114, 312-320, 1992

[25]   M.P. Wernet, M.M. Bright, G.J. Skoch, "*An Investigation of Surge in a High-Speed Centrifugal Compressor Using Digital PIV*", ASME Journal of Turbomachinery, Vol. 123, 418-428, 2001

[26]   M. Schleer, S.J. Song, R.S. Abhari, "*Clearance Effects on the Onset of Instability in a Centrifugal Compressor*", ASME Journal of Turbomachinery, Vol. 130, 2008

[27] H. Hayami, M. Hojo, S. Aramaki, "*Flow Measurements in a Transonic Centrifugal Impeller Using a PIV*", Journal of Visualization, Vol. 5, Number 3, 255-261, 2002

[28] S. Ibaraki, T. Matsuo, T. Yokoyama, "*Investigation of Unsteady Flow Field in a Vaned Diffuser of a Transonic Centrifugal Compressor*", ASME Journal of Turbomachinery, Vol. 129, Issue 4, 686-693, 2007

[29] H. Hayami, M. Hojo, S. Aramaki, "*Flow Measurement in a Transonic Centrifugal Impeller Using a PIV*", The Visualization Society of Japan and Ohmsha, LTD, Journal of Visualization, Vol. 5, No. 3, 255-261, 2002

[30] H.E. Albrecht, M. Borys, N. Damaschke, C. Tropea, "*Laser Doppler and Phase Measurement Techniques*", ISBN 3540678387, 9783540678380, Springer 2003

[31] D.P. Towers, C.E. Towers, C.H. Buckberry, M. Reeves, "*A Colour PIV System Employing Fluorescent Particles for Two-Phase Flow Measurements*", Meas. Sci. Technol. 10, 824-830, 1999

[32] K.R. Navarra, D.C. Rabe, S.D. Fonov, L.P. Goss, C. Hah, "*The Application of Pressure- and Temperature-Sensitive Paints to an Advanced Compressor*", ASME Journal of Turbomachinery, Vol. 123, 823-829, 2001

Appendix A – Performance Analysis

A.1 Polytropic Analysis

The polytropic exponent is given by equation (A.1).

$$n = \frac{\ln \frac{p_2}{p_1}}{\ln \frac{v_1}{v_2}}$$

(A.1)

The polytropic exponent can be determined when inlet and discharge pressure and temperature is known by the thermodynamic relationship given in equation (A.2).

$$\frac{T_2}{T_1} = \left(\frac{p_2}{p_1} \right)^{\left(\frac{n-1}{n} \right)}$$

(A.2)

The efficiency can be calculated when suction and discharge pressure and temperature is known, as shown in equation (A.3).

$$\eta_p = \frac{\kappa - 1}{\kappa} \frac{\ln \left(\frac{p_2}{p_1} \right)}{\ln \left(\frac{T_2}{T_1} \right)}$$

(A.3)

In cases of known polytropic efficiency, equation (A.4) can be utilized to determine the polytropic exponent.

$$\eta_p = \frac{\kappa - 1}{\kappa} \frac{n}{n - 1}$$

(A.4)

A.2 Schultz Polytropic Analysis

Compressibility functions X and Y are included in the procedure to supplement the compressibility factor Z for changes in fluid properties. When utilizing the compressibility functions in the performance analysis, the polytropic head and efficiency are determined explicitly from the performance equations. Values for the compressibility factors can be obtained from Schultz's compressibility charts. The definitions of X and Y is shown in equation (A.5) and equation (A.6).

$$X = \frac{T}{v}\left(\frac{dv}{dT}\right)_P - 1 \tag{A.5}$$

$$Y = -\frac{p}{v}\left(\frac{dv}{dp}\right)_T \tag{A.6}$$

Schultz defined a polytropic relationship as shown in equation (A.7), where the Schultz polytropic volume exponent is given in equation (A.8).

$$pv^{n_v} = \text{constant} \tag{A.7}$$

$$n_v = \frac{(1+X)}{Y\left[\frac{1}{\kappa}\left(\frac{1}{\eta_p}+X\right)-\left(\frac{1}{\eta_p}-1\right)\right]} \tag{A.8}$$

A correction factor, as defined in equation (A.9), is introduced to account for the slight variation in n_v. The volume corrected isentropic exponent is given in equation (A.10).

$$f = \frac{(\kappa_v - 1)(h_{2s} - h_1)}{\kappa_v (p_2 v_{2s} - p_1 v_1)} \tag{A.9}$$

$$\kappa_v = \frac{\kappa}{Y} \tag{A.10}$$

Schultz polytropic head becomes as shown in equation (A.11).

$$H_{p,S} = f\left[\frac{n_v}{n_v - 1}\right]\left[p_2 v_2 - p_1 v_1\right]$$ (A.11)

By introducing equation (A.7) and pv=RT in combination with equation (A.11), Schultz polytropic head becomes as shown in equation (A.12).

$$H_{p,S} = f * Z_1 R T_1\left[\frac{n_v}{n_v - 1}\right]\left[\left(\frac{p_2}{p_1}\right)^{\left(\frac{n_v - 1}{n_v}\right)} - 1\right]$$ (A.12)

The polytropic head determined from equation (A.11) and equation (A.12) is only equal if the polytropic volume exponent is defined as in equation (A.1).

A.3 Polytropic Exponent

When Schultz compressibility functions X and Y approach respectively zero and one, Schultz polytropic exponent approach the ideal polytropic exponent.

Ideal Polytropic exponent, deduced from equation (A.4):

$$n = \frac{\kappa \eta_p}{1 - \kappa + \kappa \eta_p}$$

Schultz polytropic exponent:

$$n_v = \frac{(1 + X)}{Y\left[\dfrac{1}{\kappa}\left(\dfrac{1}{\eta_p} + X\right) - \left(\dfrac{1}{\eta_p} - 1\right)\right]}$$

X = 0
Y = 1

$$n_v = \frac{(1+0)}{1*\left[\dfrac{1}{\kappa}\left(\dfrac{1}{\eta_p} + 0\right) - \left(\dfrac{1}{\eta_p} - 1\right)\right]} = \frac{1}{\left[\dfrac{1}{\kappa \eta_p} - \left(\dfrac{1 - \eta_p}{\eta_p}\right)\right]} = \frac{\kappa \eta_p}{1 - \kappa\left(1 - \eta_p\right)} = \frac{\kappa \eta_p}{1 - \kappa + \kappa \eta_p}$$

Appendix B – Verification of Discharge Coefficient and Expansibility Factor

Discharge Coefficient

The Reader-Harris/Gallagher equation for calculating the discharge coefficient is given in equation (B.1). [53]

$$C = 0,5961 + 0,0261\beta^2 - 0,216\beta^8 + 0,000521\left(\frac{10^6\beta}{Re_D}\right)^{0,7}$$

$$+ \left(0,0188 + 0,0063A\right)\beta^{3,5}\left(\frac{10^6}{Re_D}\right)^{0,3} + \left(0,043 + 0,080e^{-10L_1} - 0,123e^{-7L_1}\right)\left(1 - 0,11A\right)\frac{\beta^4}{1-\beta^4}$$

$$-0,031\left(M_2 - 0,8M_2^{1,1}\right)\beta^{1,3}$$

$$(B.1)$$

L_1 (l_1/d) and L_2 (l_2/d) are the quotients of the distance from the upstream and downstream tapping to the upstream and downstream face of the plate and pipe diameter. Due to the orifice corner tapping utilized in the compressor test these quotients become zero. M_2 (($2L_2$)/($1-\beta$)) will in addition be zero as a consequence of the corner tapping. The simplified Reader-Harris/Gallagher equation is given in equation (B.2).

$$C = 0,5961 + 0,0261\beta^2 - 0,216\beta^8 + 0,000521\left(\frac{10^6\beta}{Re_D}\right)^{0,7}$$

$$+ \left(0,0188 + 0,0063A\right)\beta^{3,5}\left(\frac{10^6}{Re_D}\right)^{0,3} + \left(0,043 + 0,080*1 - 0,123*1\right)\left(1 - 0,11A\right)\frac{\beta^4}{1-\beta^4}$$

$$(B.2)$$

The discharge coefficient is calculated for an orifice with beta value 0.6401 and for an orifice with beta value 0.4018. The discharge coefficients are estimated at maximal and minimal mass flow rate to show the effect of varying Reynolds number. The calculated values are given in Table B.1.

Table B.1: Discharge coefficients for orifices

β	0,6401	[-]
P	1,19	[kg/m^3]
D_{pipe}	0,25	[m]
A_{pipe}	0,05	[m^2]
M	0,02	[cp]
m_{max}	3,00	[kg/s]
Q_{max}	2,52	[m^3/s]
Re_{max}	763943,73	[-]
C	0,606	[-]
m_{min}	1,20	[kg/s]
Q_{min}	1,01	[m^3/s]
Re_{min}	305577,49	[-]
C	0,607	[-]

β	0,4018	[-]
ρ	1,19	[kg/m^3]
D_{pipe}	0,25	[m]
A_{pipe}	0,05	[m^2]
μ	0,02	[cp]
m_{max}	1,10	[kg/s]
Q_{max}	0,92	[m^3/s]
Re_{max}	280112,70	[-]
C	0,602	[-]
m_{min}	0,50	[kg/s]
Q_{min}	0,42	[m^3/s]
Re_{min}	127323,95	[-]
C	0,603	[-]

Expansibility Factor

Equation (B.3) shows the empirical formula for computing the expansibility factor, where *(p₂/p₁)* denotes the pressure drop over the orifice. The calculated values are given in Table B.2.The expansibility factor is calculated for an orifice with beta value 0.6401 and for an orifice with beta value 0.4018.

$$\varepsilon = 1 - \left(0,351 + 0,256\beta^4 + 0,93\beta^8\right)\left[1 - \left(\frac{p_2}{p_1}\right)^{1/\kappa}\right]$$ (B.3)

Table B.2: Expansibility factors for orifices

β	0,6401	[-]	β	0,4018	[-]
P	1,19	[kg/m³]	ρ	1,19	[kg/m³]
K	1,40	[-]	κ	1,40	[-]
m_{max}	3,00	[kg/s]	m_{max}	1,10	[kg/s]
Q_{max}	2,52	[m³/s]	Q_{max}	0,92	[m³/s]
Diff pressure	250,00	[millibar]	Diff pressure	250,00	[millibar]
P_2/p_1 (orifice)	0,75	[-]	p_2/p_1 (orifice)	0,75	[-]
E	0,922	[-]	E	0,934	[-]
m_{min}	1,20	[kg/s]	m_{min}	0,50	[kg/s]
Q_{min}	1,01	[m³/s]	Q_{min}	0,42	[m³/s]
Diff pressure	34,52	[millibar]	Diff pressure	45,98	[millibar]
p_2/p_1 (orifice)	0,97	[-]	p_2/p_1 (orifice)	0,95	[-]
ε	0,990	[-]	ε	0,988	[-]

Appendix C – PRO/II Setup

Stream Name		SUCTION	DISCHARGE
Temperature	K	295,000	331,956
Pressure	BAR	0,960	1,376
Flowrate	KG-MOL/SEC	0,017	0,017

Vapor CP/CV Ratio		1,4039	1,4032
Vapor Act. Vol. Rate	m3/sec	0,4234	0,3324

Compressor Name		COMPRESSOR
Compressor Description		
Pressure	BAR	1,3761
Temperature	K	331,9560
Head	M	3771,3159
Actual Work	KW	17,7584
Isentropic coef., k		1,4031
Comp Polytropic Coefficient		1,5594

DISCHARGE

COMPRESSOR

SUCTION

89
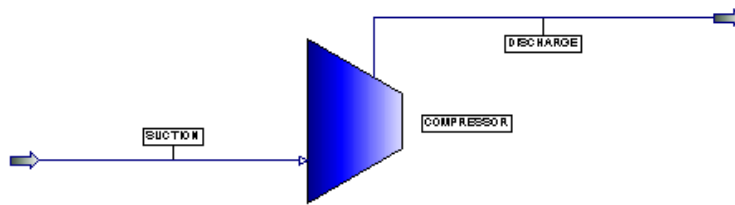
Appendix D – Schultz Generalized Compressibility Charts
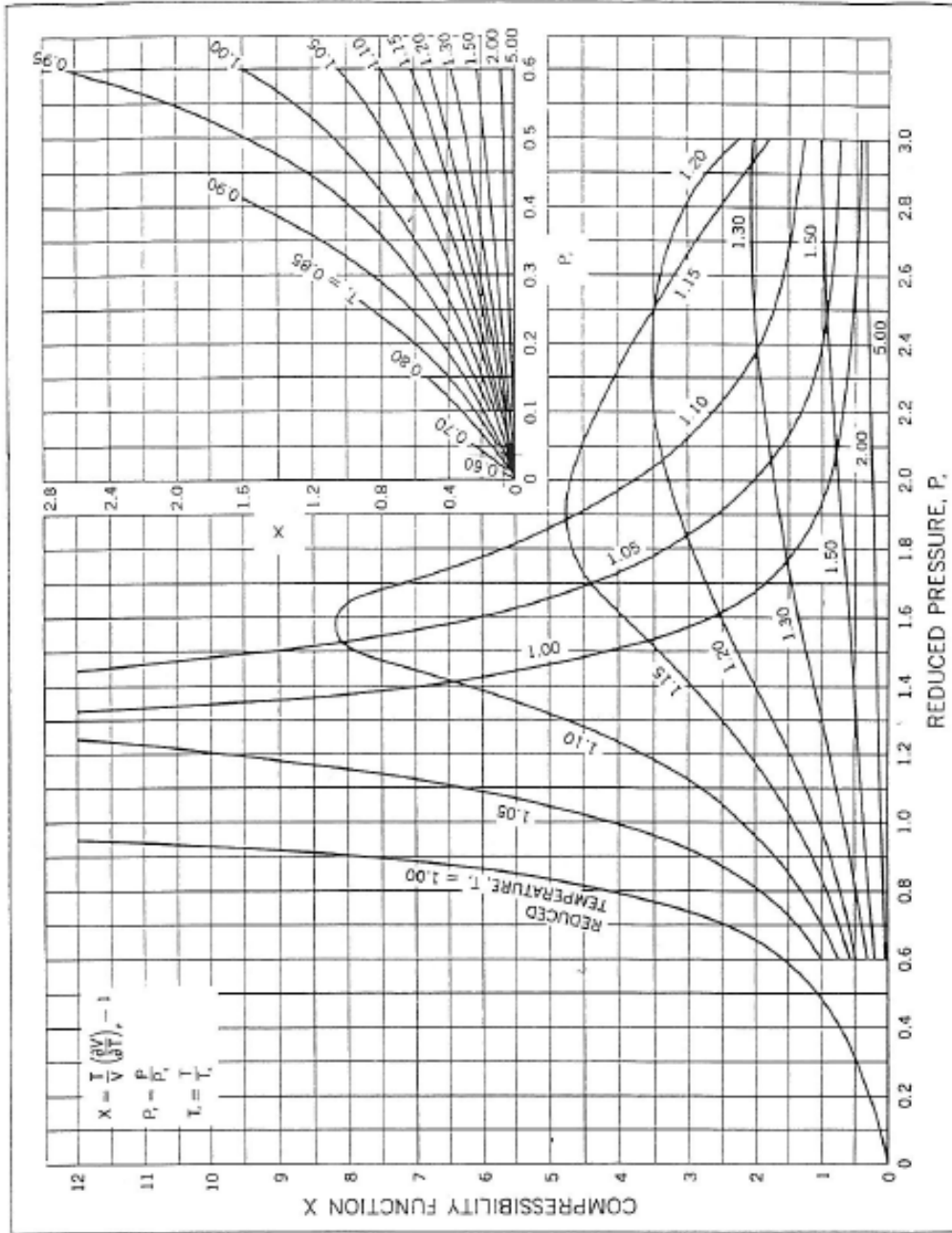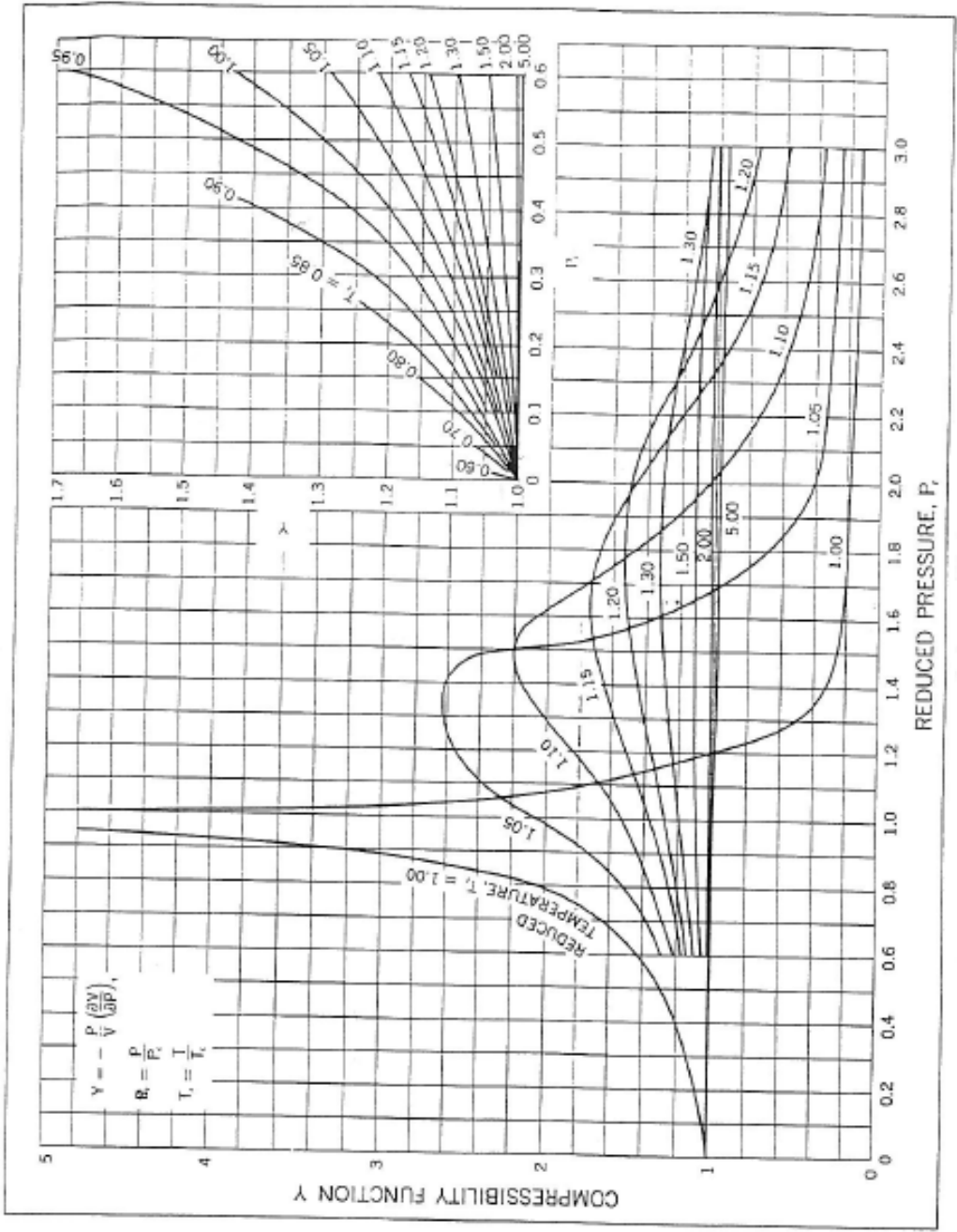
Appendix E – Valid Test Points

	Test Point	
	Temperature Discharge, T2	29,73
Test Interval 11	Temperature Inlet, T1	23,05
	Pressure Discharge, p2	1,00
	Pressure Inlet, p1	0,94
	Speed	4983,21
	Test Point	
	Temperature Discharge, T2	29,76
Test Interval 12	Temperature Inlet, T1	23,08
	Pressure Discharge, p2	1,00
	Pressure Inlet, p1	0,94
	Speed	4941,49
	Test Point	
	Temperature Discharge, T2	29,82
Test Interval 13	Temperature Inlet, T1	23,12
	Pressure Discharge, p2	1,00
	Pressure Inlet, p1	0,94
	Speed	4989,98
	Test Point	
	Temperature Discharge, T2	30,28
Test Interval 25	Temperature Inlet, T1	23,38
	Pressure Discharge, p2	1,01
	Pressure Inlet, p1	0,94
	Speed	4950,66
	Test Point	
	Temperature Discharge, T2	30,67
Test Interval 35	Temperature Inlet, T1	23,49
	Pressure Discharge, p2	1,02
	Pressure Inlet, p1	0,95
	Speed	4937,28
	Test Point	
	Temperature Discharge, T2	30,68
Test Interval 37	Temperature Inlet, T1	23,48
	Pressure Discharge, p2	1,02
	Pressure Inlet, p1	0,95
	Speed	4947,21
	Test Point	
	Temperature Discharge, T2	31,05
Test Interval 44	Temperature Inlet, T1	23,50
	Pressure Discharge, p2	1,06
	Pressure Inlet, p1	0,97
	Speed	4948,18

	Test Point	
	Temperature Discharge, T2	31,08
Test Interval 46	Temperature Inlet, T1	23,45
	Pressure Discharge, p2	1,06
	Pressure Inlet, p1	0,97
	Speed	4957,66
	Test Point	
	Temperature Discharge, T2	31,11
Test Interval 47	Temperature Inlet, T1	23,45
	Pressure Discharge, p2	1,06
	Pressure Inlet, p1	0,97
	Speed	4939,39
	Test Point	
	Temperature Discharge, T2	31,31
Test Interval 55	Temperature Inlet, T1	23,57
	Pressure Discharge, p2	1,07
	Pressure Inlet, p1	0,98
	Speed	4951,19
	Test Point	
	Temperature Discharge, T2	31,35
Test Interval 56	Temperature Inlet, T1	23,57
	Pressure Discharge, p2	1,08
	Pressure Inlet, p1	0,98
	Speed	4953,22
	Test Point	
	Temperature Discharge, T2	31,41
Test Interval 60	Temperature Inlet, T1	23,54
	Pressure Discharge, p2	1,09
	Pressure Inlet, p1	0,99
	Speed	4965,77
	Test Point	
	Temperature Discharge, T2	31,48
Test Interval 62	Temperature Inlet, T1	23,56
	Pressure Discharge, p2	1,09
	Pressure Inlet, p1	0,99
	Speed	4938,86

Appendix F – Computation of Non-Dimensional Head and Flow Coefficients

Table F.1: Calculation of performance parameters at test condition

Test Point	Measured		Calculated		
	Q_1 [m³/s]	N [rpm]	H_p [J/kg]	ψ_p [-]	φ [-]
11	0,83	4983	5505	0,55	0,0279
25	0,81	4951	5863	0,59	0,0274
35	0,77	4937	6430	0,65	0,0261
44	0,6	4948	7772	0,78	0,0203
55	0,54	4951	8045	0,81	0,0183
60	0,41	4966	8447	0,84	0,0138

Appendix G – Measurement Sensitivity Analysis

G.1 Measurement sensitivity for case 1

Inlet Pressure

Table G.1: Measurement sensitivity with varying inlet pressure – Case 1

				Inlet Pressure, p_1			
p_1 [bar]	Deviation p_1 [bar]	Deviation p_1 [%]	n [-]	H_p [J/kg]	Deviation Hp [%]	η_p [-]	Deviation η_p [%]
0,940	-0,010	-1,05	1,48	6156	17,3	0,88	17,3
0,941	-0,009	-0,95	1,50	6062	15,5	0,86	15,5
0,942	-0,008	-0,84	1,51	5971	13,8	0,85	13,8
0,943	-0,007	-0,74	1,52	5880	12,1	0,84	12,1
0,944	-0,006	-0,63	1,53	5789	10,3	0,82	10,4
0,945	-0,005	-0,53	1,54	5699	8,6	0,81	8,6
0,946	-0,004	-0,42	1,56	5608	6,9	0,80	6,9
0,947	-0,003	-0,32	1,57	5517	5,2	0,78	5,2
0,948	-0,002	-0,21	1,59	5427	3,4	0,77	3,4
0,949	-0,001	-0,11	1,60	5337	1,7	0,76	1,7
0,950	**0,000**	**0,00**	**1,62**	**5246**	**0,0**	**0,75**	**0,0**
0,951	0,001	0,11	1,64	5156	-1,7	0,73	-1,7
0,952	0,002	0,21	1,66	5066	-3,4	0,72	-3,4
0,953	0,003	0,32	1,68	4976	-5,1	0,71	-5,1
0,954	0,004	0,42	1,70	4887	-6,9	0,69	-6,9
0,955	0,005	0,53	1,72	4797	-8,6	0,68	-8,6
0,956	0,006	0,63	1,74	4707	-10,3	0,67	-10,3
0,957	0,007	0,74	1,77	4618	-12,0	0,66	-12,0
0,958	0,008	0,84	1,80	4528	-13,7	0,64	-13,7
0,959	0,009	0,95	1,83	4439	-15,4	0,63	-15,4
0,960	0,010	1,05	1,86	4349	-17,1	0,62	-17,1

Outlet Pressure

Table G.2: Measurement sensitivity with varying outlet pressure – Case 1

	Outlet Pressure, p_2						
p_2 [bar]	Deviation p_2 [bar]	Deviation p_2 [%]	n [-]	H_p [J/kg]	Deviation Hp [%]	η_p [-]	Deviation η_p [%]
1,000	-0,010	-0,990	1,84	4396	-16,2	0,62	-16,2
1,001	-0,009	-0,891	1,81	4480	-14,6	0,64	-14,6
1,002	-0,008	-0,792	1,79	4565	-13,0	0,65	-13,0
1,003	-0,007	-0,693	1,76	4651	-11,4	0,66	-11,4
1,004	-0,006	-0,594	1,74	4736	-9,7	0,67	-9,7
1,005	-0,005	-0,495	1,71	4821	-8,1	0,69	-8,1
1,006	-0,004	-0,396	1,69	4907	-6,5	0,70	-6,5
1,007	-0,003	-0,297	1,67	4992	-4,9	0,71	-4,9
1,008	-0,002	-0,198	1,65	5077	-3,2	0,72	-3,2
1,009	-0,001	-0,099	1,64	5162	-1,6	0,73	-1,6
1,010	**0,000**	**0,000**	**1,62**	**5246**	**0,0**	**0,75**	**0,0**
1,011	0,001	0,099	1,60	5331	1,6	0,76	1,6
1,012	0,002	0,198	1,59	5416	3,2	0,77	3,2
1,013	0,003	0,297	1,58	5501	4,8	0,78	4,8
1,014	0,004	0,396	1,56	5585	6,5	0,79	6,5
1,015	0,005	0,495	1,55	5670	8,1	0,81	8,1
1,016	0,006	0,594	1,54	5754	9,7	0,82	9,7
1,017	0,007	0,693	1,52	5838	11,3	0,83	11,3
1,018	0,008	0,792	1,51	5922	12,9	0,84	12,9
1,019	0,009	0,891	1,50	6006	14,5	0,85	14,5
1,020	0,010	0,990	1,49	6090	16,1	0,87	16,1

Inlet Temperature

Table G.3: Measurement sensitivity with varying inlet temperature – Case 1

	Inlet Temperature, T_1						
T_1 [K]	Deviation T_1 [K]	Deviation T_1 [%]	n [-]	H_p [J/kg]	Deviation H_p [%]	η_p [-]	Deviation η_p [%]
290,0	-5,0	-1,69	2,96	5202	-0,85	0,43	-42,2
290,5	-4,5	-1,53	2,73	5207	-0,76	0,45	-39,6
291,0	-4,0	-1,36	2,54	5211	-0,68	0,47	-36,8
291,5	-3,5	-1,19	2,37	5215	-0,59	0,49	-33,7
292,0	-3,0	-1,02	2,22	5220	-0,51	0,52	-30,4
292,5	-2,5	-0,85	2,09	5224	-0,42	0,55	-26,6
293,0	-2,0	-0,68	1,98	5229	-0,34	0,58	-22,5
293,5	-1,5	-0,51	1,87	5233	-0,25	0,61	-17,9
294,0	-1,0	-0,34	1,78	5238	-0,17	0,65	-12,6
294,5	-0,5	-0,17	1,70	5242	-0,08	0,70	-6,7
295,0	**0,0**	**0,00**	**1,62**	**5246**	**0,00**	**0,75**	**0,0**
295,5	0,5	0,17	1,55	5251	0,08	0,80	7,8
296,0	1,0	0,34	1,49	5255	0,17	0,87	16,9
296,5	1,5	0,51	1,43	5260	0,25	0,95	27,6
297,0	2,0	0,68	1,37	5264	0,34	1,05	40,5
297,5	2,5	0,85	1,32	5269	0,42	1,17	56,2
298,0	3,0	1,02	1,28	5273	0,51	1,31	75,9
298,5	3,5	1,19	1,24	5277	0,59	1,50	101,2
299,0	4,0	1,36	1,19	5282	0,67	1,75	134,9
299,5	4,5	1,53	1,16	5286	0,76	2,11	182,1
300,0	5,0	1,69	1,12	5291	0,84	2,63	253,0

Outlet Temperature

Table G.4: Measurement sensitivity with varying outlet temperature – Case 1

Outlet Temperature, T_2							
T_2 [K]	Deviation T_2 [K]	Deviation T_2 [%]	n [-]	H_p [J/kg]	Deviation, H_p [%]	η_p [-]	Deviation, η_p [%]
297,0	-5,0	-1,66	1,12	5203	-0,83	2,59	247,1
297,5	-4,5	-1,49	1,16	5207	-0,75	2,07	177,8
298,0	-4,0	-1,32	1,20	5212	-0,67	1,73	131,7
298,5	-3,5	-1,16	1,24	5216	-0,58	1,48	98,8
299,0	-3,0	-0,99	1,28	5220	-0,50	1,30	74,1
299,5	-2,5	-0,83	1,33	5225	-0,42	1,16	54,9
300,0	-2,0	-0,66	1,38	5229	-0,33	1,04	39,5
300,5	-1,5	-0,50	1,43	5233	-0,25	0,95	26,9
301,0	-1,0	-0,33	1,49	5238	-0,17	0,87	16,5
301,5	-0,5	-0,17	1,55	5242	-0,08	0,80	7,6
302,0	**0,0**	**0,00**	**1,62**	**5246**	**0,00**	**0,75**	**0,0**
302,5	0,5	0,17	1,69	5251	0,08	0,70	-6,6
303,0	1,0	0,33	1,78	5255	0,17	0,65	-12,3
303,5	1,5	0,50	1,87	5260	0,25	0,62	-17,4
304,0	2,0	0,66	1,96	5264	0,33	0,58	-21,9
304,5	2,5	0,83	2,07	5268	0,41	0,55	-26,0
305,0	3,0	0,99	2,19	5273	0,50	0,52	-29,6
305,5	3,5	1,16	2,33	5277	0,58	0,50	-32,9
306,0	4,0	1,32	2,49	5281	0,66	0,48	-35,9
306,5	4,5	1,49	2,66	5286	0,75	0,46	-38,7
307,0	5,0	1,66	2,87	5290	0,83	0,44	-41,2

G.2 Measurement sensitivity for case 2

Inlet Pressure

Table G.5: Measurement sensitivity with varying inlet pressure – Case 2

Inlet Pressure, P_1							
p_1 [bar]	Deviation p_1 [bar]	Deviation p_1 [%]	n [-]	H_p [J/kg]	Deviation Hp [%]	η_p [-]	Deviation η_p [%]
0,940	-0,010	-1,053	1,56	73479	1,5	0,79	0,9
0,941	-0,009	-0,947	1,56	73338	1,3	0,79	0,8
0,942	-0,008	-0,842	1,56	73235	1,1	0,79	0,7
0,943	-0,007	-0,737	1,57	73131	1,0	0,79	0,5
0,944	-0,006	-0,632	1,57	73028	0,9	0,79	0,4
0,945	-0,005	-0,526	1,57	72925	0,7	0,79	0,2
0,946	-0,004	-0,421	1,57	72822	0,6	0,79	0,1
0,947	-0,003	-0,316	1,57	72720	0,4	0,79	-0,1
0,948	-0,002	-0,211	1,57	72617	0,3	0,79	-0,2
0,949	-0,001	-0,105	1,57	72515	0,1	0,78	-0,3
0,950	**0,000**	**0,000**	**1,57**	**72412**	**0,0**	**0,78**	**-0,5**
0,951	0,001	0,105	1,58	72310	-0,1	0,78	-0,6
0,952	0,002	0,211	1,58	72207	-0,3	0,78	-0,8
0,953	0,003	0,316	1,58	72105	-0,4	0,78	-0,9
0,954	0,004	0,421	1,58	72003	-0,6	0,78	-1,0
0,955	0,005	0,526	1,58	71901	-0,7	0,78	-1,2
0,956	0,006	0,632	1,58	71800	-0,8	0,78	-1,3
0,957	0,007	0,737	1,58	71698	-1,0	0,78	-1,5
0,958	0,008	0,842	1,58	71596	-1,1	0,77	-1,6
0,959	0,009	0,947	1,59	71495	-1,3	0,77	-1,7
0,960	0,010	1,053	1,59	71394	-1,4	0,77	-1,9

Outlet Pressure

Table G.6: Measurement sensitivity with varying outlet pressure – Case 2

Outlet Pressure, p_2							
p_2 [bar]	Deviation p_2 [bar]	Deviation p_2 [%]	n [-]	H_p [J/kg]	Deviation Hp [%]	η_p [-]	Deviation η_p [%]
1,990	-0,010	-0,500	1,58	71961	-0,6	0,78	-0,7
1,991	-0,009	-0,450	1,58	71973	-0,6	0,78	-0,6
1,992	-0,008	-0,400	1,58	72022	-0,5	0,78	-0,5
1,993	-0,007	-0,350	1,58	72071	-0,5	0,78	-0,5
1,994	-0,006	-0,300	1,58	72120	-0,4	0,78	-0,4
1,995	-0,005	-0,250	1,58	72169	-0,3	0,78	-0,3
1,996	-0,004	-0,200	1,58	72217	-0,3	0,78	-0,3
1,997	-0,003	-0,150	1,58	72266	-0,2	0,78	-0,2
1,998	-0,002	-0,100	1,58	72315	-0,1	0,78	-0,1
1,999	-0,001	-0,050	1,57	72363	-0,1	0,78	-0,1
2,000	**0,000**	**0,000**	**1,57**	**72412**	**0,0**	**0,78**	**0,0**
2,001	0,001	0,050	1,57	72461	0,1	0,78	0,1
2,002	0,002	0,100	1,57	72509	0,1	0,78	0,1
2,003	0,003	0,150	1,57	72558	0,2	0,79	0,2
2,004	0,004	0,200	1,57	72606	0,3	0,79	0,3
2,005	0,005	0,250	1,57	72655	0,3	0,79	0,3
2,006	0,006	0,300	1,57	72703	0,4	0,79	0,4
2,007	0,007	0,350	1,57	72752	0,5	0,79	0,5
2,008	0,008	0,400	1,57	72800	0,5	0,79	0,5
2,009	0,009	0,450	1,57	72849	0,6	0,79	0,6
2,010	0,010	0,500	1,57	72897	0,7	0,79	0,7

Inlet Temperature

Table G.7: Measurement sensitivity with varying inlet temperature – Case 2

Inlet Temperature, T_1							
T_1 [K]	Deviation T_1 [K]	Deviation T_1 [%]	n [-]	H_p [J/kg]	Deviation H_p [%]	η_p [-]	Deviation η_p [%]
290,0	-5,0	-1,69	1,63	71824	-0,81	0,74	-5,9
290,5	-4,5	-1,53	1,63	71883	-0,73	0,74	-5,4
291,0	-4,0	-1,36	1,62	71942	-0,65	0,75	-4,8
291,5	-3,5	-1,19	1,61	72001	-0,57	0,75	-4,2
292,0	-3,0	-1,02	1,61	72060	-0,49	0,76	-3,6
292,5	-2,5	-0,85	1,60	72119	-0,41	0,76	-3,0
293,0	-2,0	-0,68	1,60	72177	-0,32	0,76	-2,4
293,5	-1,5	-0,51	1,59	72236	-0,24	0,77	-1,8
294,0	-1,0	-0,34	1,59	72295	-0,16	0,77	-1,2
294,5	-0,5	-0,17	1,58	72353	-0,08	0,78	-0,6
295,0	**0,0**	**0,00**	**1,57**	**72412**	**0,00**	**0,78**	**0,0**
295,5	0,5	0,17	1,57	72471	0,08	0,79	0,6
296,0	1,0	0,34	1,56	72529	0,16	0,79	1,3
296,5	1,5	0,51	1,56	72588	0,24	0,80	1,9
297,0	2,0	0,68	1,55	72646	0,32	0,80	2,5
297,5	2,5	0,85	1,55	72705	0,40	0,81	3,2
298,0	3,0	1,02	1,54	72763	0,48	0,81	3,9
298,5	3,5	1,19	1,54	72821	0,57	0,82	4,5
299,0	4,0	1,36	1,53	72880	0,65	0,82	5,2
299,5	4,5	1,53	1,53	72938	0,73	0,83	5,9
300,0	5,0	1,69	1,52	72996	0,81	0,84	6,6

Outlet Temperature

Table G.8: Measurement sensitivity with varying outlet temperature – Case 2

Outlet Temperature, T_2							
T_2 [K]	Deviation T_2 [K]	Deviation T_2 [%]	n [-]	H_p [J/kg]	Deviation, H_p [%]	η_p [-]	Deviation, η_p [%]
382,0	-5,0	-1,29	1,53	71922	-0,68	0,82	5,0
382,5	-4,5	-1,16	1,54	71971	-0,61	0,82	4,5
383,0	-4,0	-1,03	1,54	72020	-0,54	0,81	4,0
383,5	-3,5	-0,90	1,54	72069	-0,47	0,81	3,5
384,0	-3,0	-0,78	1,55	72118	-0,41	0,81	2,9
384,5	-2,5	-0,65	1,55	72167	-0,34	0,80	2,4
385,0	-2,0	-0,52	1,56	72216	-0,27	0,80	1,9
385,5	-1,5	-0,39	1,56	72265	-0,20	0,79	1,4
386,0	-1,0	-0,26	1,57	72314	-0,14	0,79	1,0
386,5	-0,5	-0,13	1,57	72363	-0,07	0,79	0,5
387,0	**0,0**	**0,00**	**1,57**	**72412**	**0,00**	**0,78**	**0,0**
387,5	0,5	0,13	1,58	72461	0,07	0,78	-0,5
388,0	1,0	0,26	1,58	72510	0,13	0,78	-0,9
388,5	1,5	0,39	1,59	72559	0,20	0,77	-1,4
389,0	2,0	0,52	1,59	72607	0,27	0,77	-1,9
389,5	2,5	0,65	1,60	72656	0,34	0,77	-2,3
390,0	3,0	0,78	1,60	72705	0,40	0,76	-2,8
390,5	3,5	0,90	1,60	72754	0,47	0,76	-3,2
391,0	4,0	1,03	1,61	72803	0,54	0,75	-3,7
391,5	4,5	1,16	1,61	72851	0,61	0,75	-4,1
392,0	5,0	1,29	1,62	72900	0,67	0,75	-4,5